THE UNIVERSITY OF ALBERTA

SHAPE RESONANCES IN SUPERCONDUCTING THIN FILMS

by

D. W. Penner

A THESIS

SUBMITTED TO THE FACULTY OF GRADUATE STUDIES

IN PARTIAL FULFILMENT OF THE REQUIREMENTS FOR THE DEGREE

OF MASTER OF SCIENCE

DEPARTMENT OF PHYSICS

EDMONTON, ALBERTA

SEPTEMBER, 1964

UNIVERSITY OF ALBERTA

FACULTY OF GRADUATE STUDIES

The undersigned certify that they have read, and recommend to the Faculty of Graduate Studies for acceptance, a thesis entitled SHAPE RESONANCES IN SUPERCONDUCTING THIN FILMS, submitted by D. W. Penner, in partial fulfilment for the degree of Master of Science.

ACKNOWLEDGEMENTS

I wish to thank

Dr. S.B. Woods, my research supervisor, for suggesting the project and for his patient help and encouragement,

Dr. J.S. Rogers, for many valuable suggestions, and for assistance in operating the He^3 cryostat,

the National Research Council, for financial support of the project, which was greatly appreciated,

and finally

members of the technical staff, who supplied liquid air and liquid helium and assisted or advised with a number of problems that were encountered.

ABSTRACT

In 1963, Blatt and Thompson predicted the occurrence of "shape resonances" in the superconducting energy gap as a function of thickness in thin films. Investigation of this effect shows no definite evidence to prove or disprove this theory. The results are, however, easily explained as being due to the differential contraction of an aluminum film and a glass substrate cooled from room temperature to 1°K.

The broadening of the superconducting gap-edge singularity was also investigated and it is found that the mechanism causing the broadening is independent of temperature in the range 0.3 to 1°K. It was also found that the current due to thermally excited electrons in a tunnel junction is a reliable indicator of the junction temperature.

TABLE OF CONTENTS

LIST OF TABLES

LIST OF FIGURES

CHAPTER I

INTRODUCTION

This thesis reports on an extension of the electron tunneling work begun in this laboratory by Adler (1963) and Rogers (1964). The tunnel junctions used here are made of two thin metal strips in the form of a cross and separated from one another by a thin dielectric barrier layer. The experiments consist essentially of a four terminal measurement of the current-voltage (I-V) characteristic of the junction with either one or both of the metal layers in the superconducting state. All the specimens for the present work consisted of aluminum layers separated by aluminum oxide barrier layers.

The general shape of the current-voltage characteristic of a tunnel junction can be easily deduced from the density of states of the metals forming the junction by using a simple single particle model of the tunneling process. Figure 1 shows the density of states close to the Fermi level plotted against energy on the ordinate for the three cases of neither, one, or both metal layers in the superconducting state. Also shown is the corresponding current-voltage characteristic. All cases are considered at a temperature T greater than 0° K.

FIGURE 1

Schematic description of various tunneling processes. This figure shows the density of states, D(E), near the Fermi surface plotted against energy, E. The corresponding current-voltage curves are also shown.

(a) Both films normal

(b) One film superconducting

(c) Both films superconducting

(a)

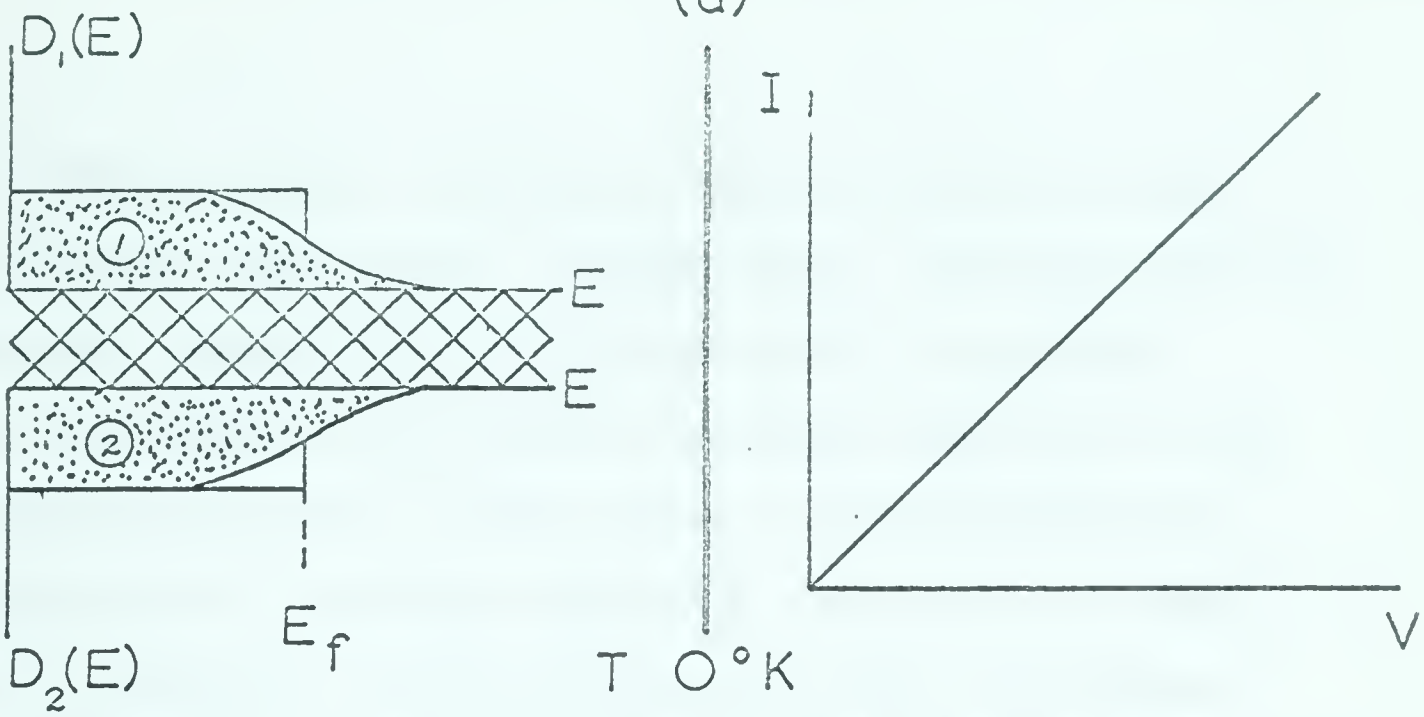
D₁(E)
1
E
E
2
E_f
D₂(E)
I
V
T O°K

(b)

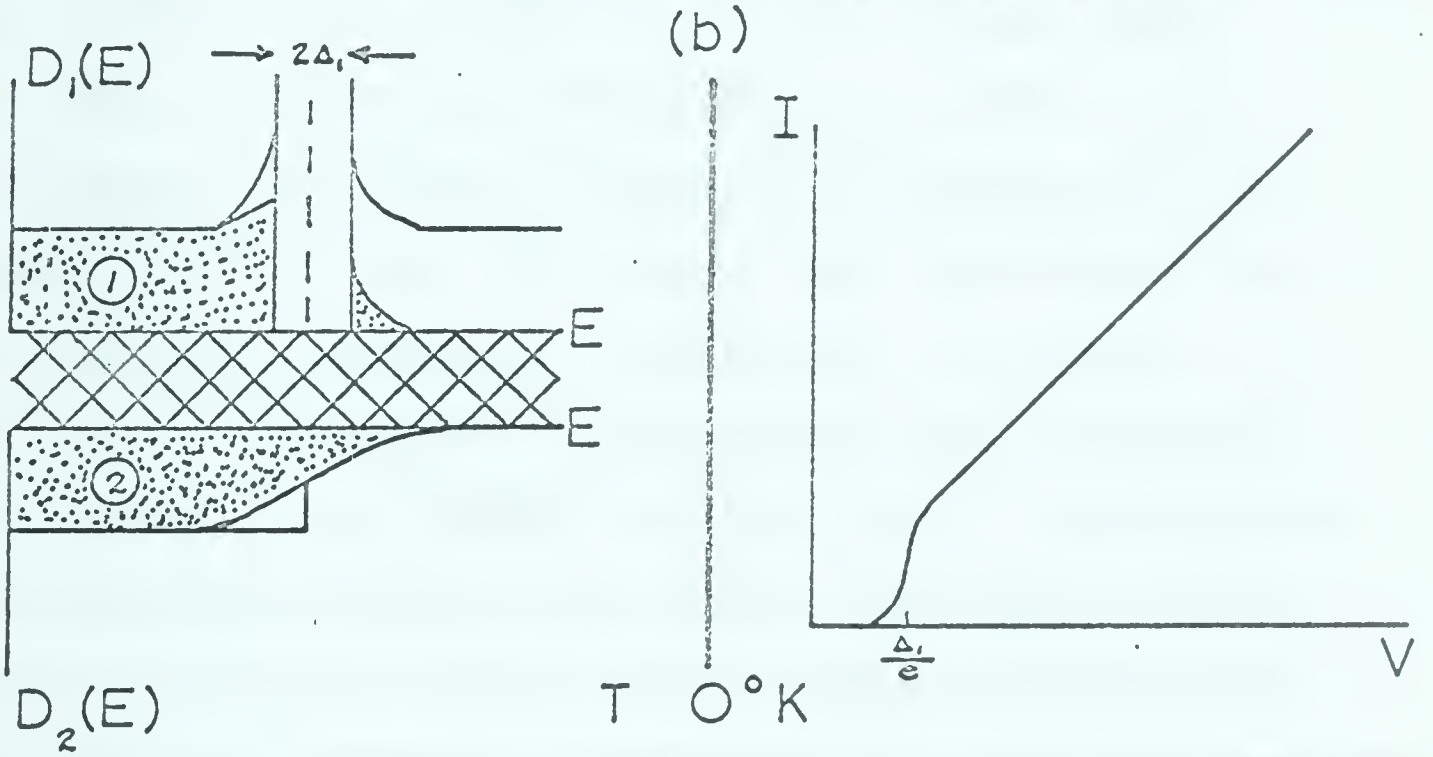
D₁(E)
2Δ₁
1
E
E
2
D₂(E)
I
V
Δ₁/e
T O°K

(c)

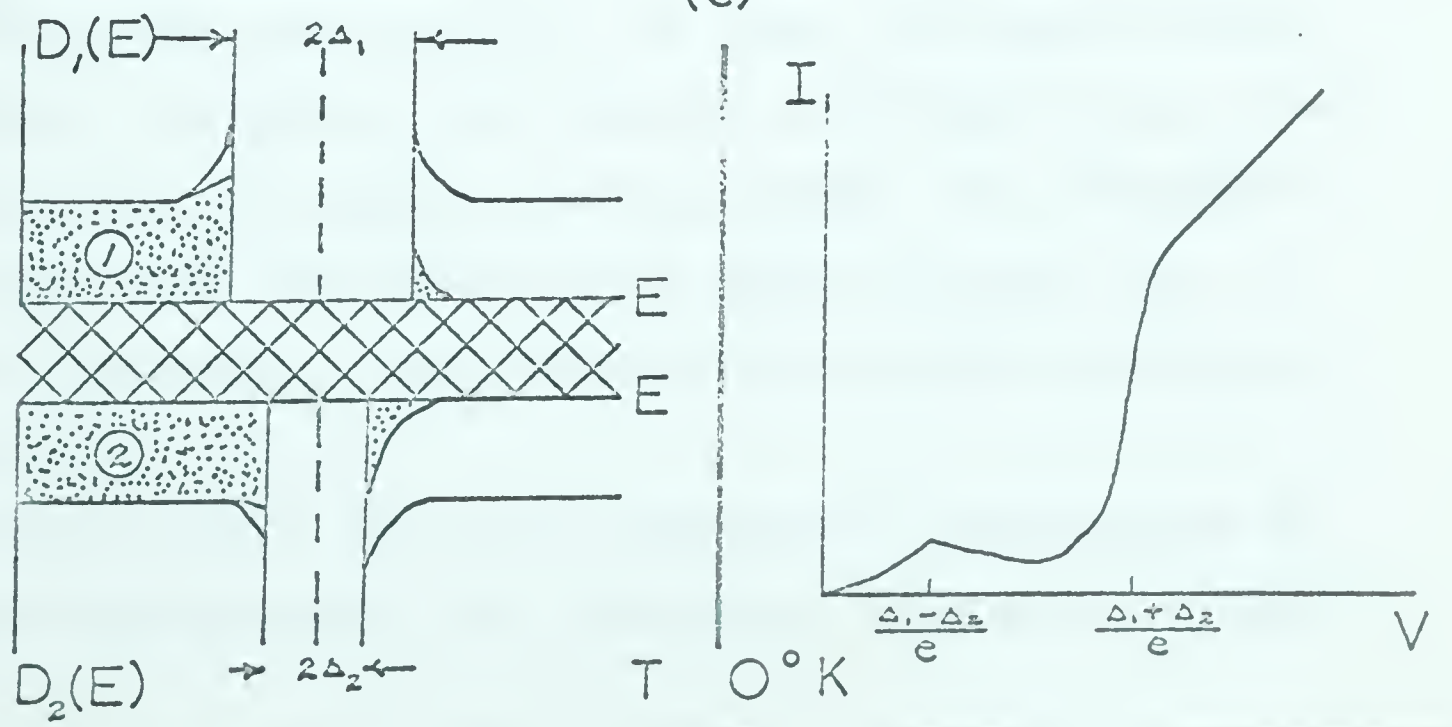
D₁(E)
2Δ₁
1
E
E
2
D₂(E)
2Δ₂
I
V
Δ₁−Δ₂/e
Δ₁+Δ₂/e
T O°K

In Figure 1(a) a junction is shown with both metal layers in the normal state. In this case, for small applied voltages the current varies linearly with the applied voltage. In Figure 1(b), one of the metal layers is in the superconducting state. In this case, the superconducting energy gap makes tunneling impossible (except for a small number of thermally excited electrons) until the applied voltage reaches a value equal to one half the gap width. At this point, the current rises rapidly as shown in the diagram. Figure 1(c) shows the density of states and I-V characteristic when both metal layers are superconducting and when different metals are used so that $\Delta_1 \neq \Delta_2$. The cusp in the I-V characteristic occurs when the applied voltage reaches $V = \frac{\Delta_1 - \Delta_2}{e}$ so that all of the thermally excited electrons in metal 2 can tunnel into metal 1. For a further increase in applied voltage these electrons face a lower available density of states and since the number of electrons which can tunnel is the same, the tunnel current decreases, resulting in the negative resistance region shown. Finally, when the applied voltage reaches $V = \frac{\Delta_1 + \Delta_2}{e}$, electrons below the energy gap in metal 2 are now free to tunnel into metal 1, resulting in a very rapid increase in current.

The principal aim of the experiments reported here is to check experimentally the theoretical prediction by Blatt

and Thompson (1963 a,b) that the superconducting energy gap in a thin film is a periodic function of the film thickness. Tunneling experiments are ideal for this purpose since one normally uses fairly thin films in them. Moreover, according to Blatt and Thompson, one should be able to obtain the current-voltage characteristic corresponding to two different superconducting metals merely by using different thicknesses of the same metal. If one of the metal layers is made thick enough to behave like bulk material, we have a direct indication of whether or not the superconducting energy gap in a thin film is different from the bulk value.

A secondary objective of the present experiments was to extend the work, begun by Rogers (1964), on the use of tunnel junctions as thermometers. The basis for this work is easily seen from the current-voltage characteristic in Figure 1(c). At point A, the tunnel current is due entirely to thermally excited electrons in metal 2. Since this current depends on the number of thermally excited electrons available, which in turn depends on the temperature, the size of the current flowing at this point should be a good measure of the temperature of the tunnel junction.

If possible, it was also intended to make a systematic study of the temperature and thickness dependence of the broadening of the gap-edge singularity as exhibited by the

I-V characteristics of tunnel junctions. An explanation of the origin of this broadening can be given with the help of Figure 2, which shows the density of states diagrams and corresponding I-V characteristics for a junction with both metal layers superconducting at $T = 0^\circ K$, and at $T > 0^\circ K$. In Figure 2(a), ($T = 0^\circ K$), there are no thermally excited electrons. Hence the cusp at $V = \frac{\Delta_1 - \Delta_2}{e}$ is absent and the current displays a finite jump at $V = \frac{\Delta_1 + \Delta_2}{e}$. However, at temperatures above $0^\circ K.$, there are thermally excited electrons which lead to the cusp and negative resistance region and which also give a finite slope to the current jump at $V = \frac{\Delta_1 + \Delta_2}{e}$. This effect is said to be due to "kT smearing" of the superconducting energy gap. Earlier workers (Giaever, et al, 1962; Adler, 1963) found that the actual slope of the I-V characteristic was smaller than could be accounted for by this effect alone, and attributed their results to a "smearing" of the superconducting density of states at the gap edge, doing away with the infinite singularity in the density of states as given by the BCS theory. The variation of the slope of the I-V characteristic at $V = \frac{\Delta_1 + \Delta_2}{e}$ was examined to determine whether or not the appropriateness of the various theoretical methods of introducing smearing into the BCS function could be judged from such experimental results.

FIGURE 2

Schematic description of tunneling process between two superconductors at T=0°K, and at T > 0°K, illustrating the origin of "kT smearing". The corresponding current-voltage curves are also shown.

(a) T = 0° K

(b) T > 0° K

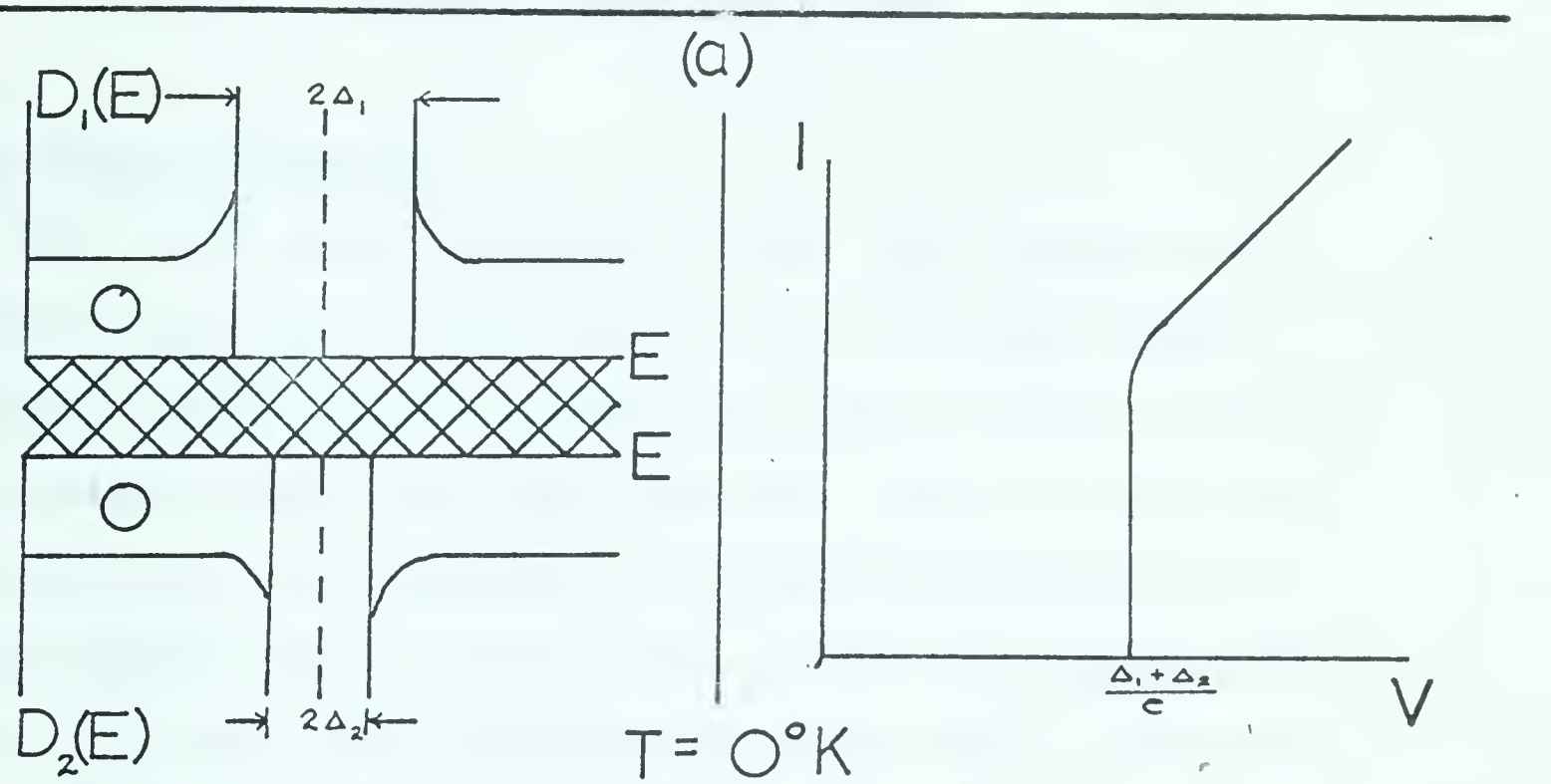
(a)
$D_1(E)$
$2\Delta_1$
E
E
$D_2(E)$
$2\Delta_2$
I
V
$\frac{\Delta_1+\Delta_2}{e}$
T = 0°K

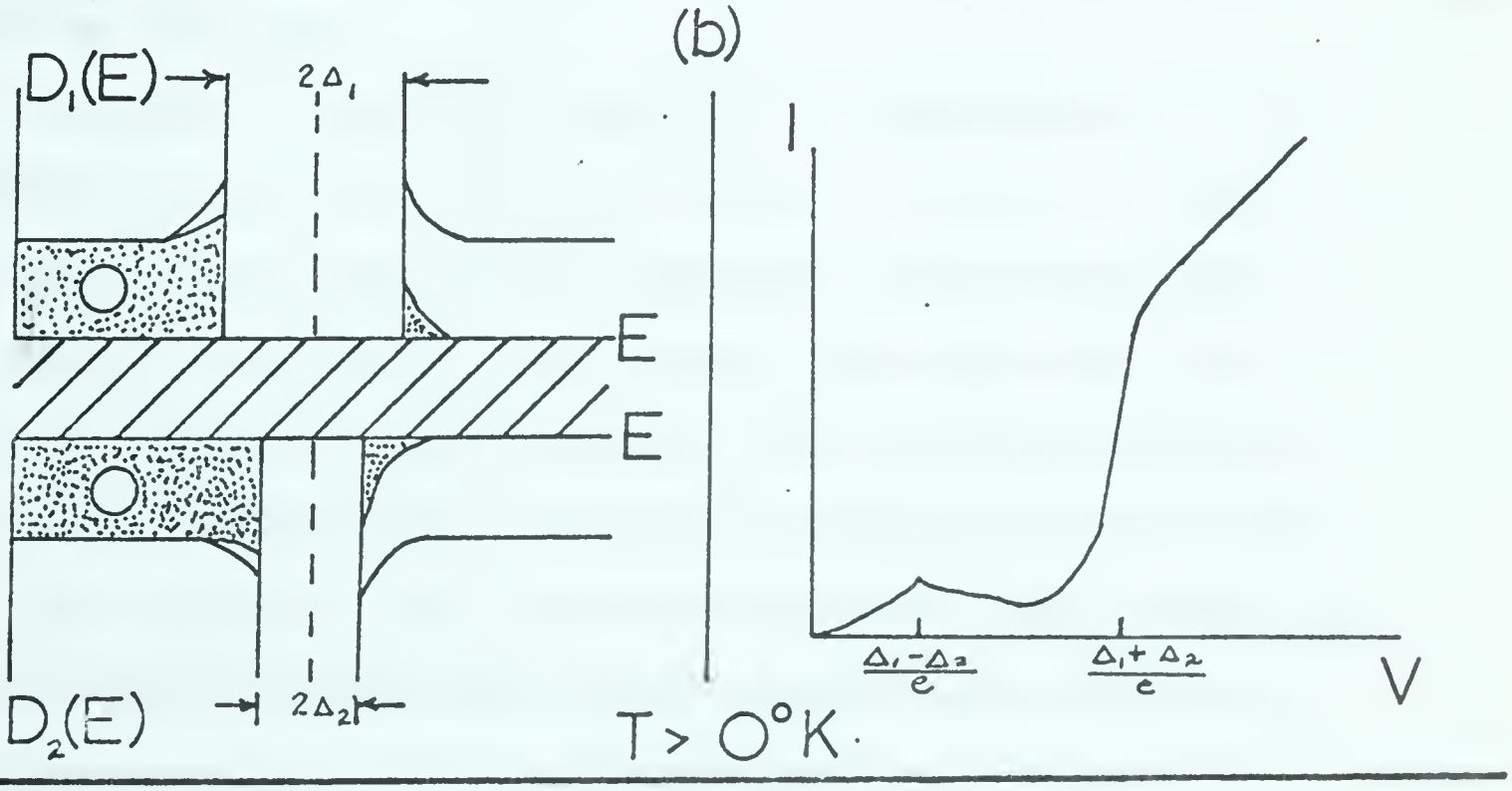
(b)
$D_1(E)$
$2\Delta_1$
E
E
$D_2(E)$
$2\Delta_2$
I
V
$\frac{\Delta_1-\Delta_2}{e}$
$\frac{\Delta_1+\Delta_2}{e}$
T > 0°K.

CHAPTER II

EXPERIMENTAL TECHNIQUES

A. Specimen Preparation

The tunnel junctions used in this work consisted of evaporated aluminum layers separated by an oxide layer. In short, a base layer is evaporated onto a glass substrate, and allowed to oxidize. Then the cover layer, in this case the thin film, is deposited. The method is described in greater detail below, and by Adler (1963) and Rogers (1964), who used the same general method although with a different oxidation technique.

The glass substrates used are one centimeter by 2.5 centimeter pieces of microscope slide. To ensure a clean substrate, it is washed with detergent, drip-dried, and then flamed in a Bunsen burner until the edges are fire-polished. Indium is then smeared on the slide at the positions of the prospective electrical contacts. It was found with some specimens that the leads could be indium-soldered to the substrate after the tunnel junction was completed. However, in most attempts to follow this procedure either the indium would not wet the glass or a good indium-aluminum contact could not be obtained. However, if the indium is smeared on the substrate before any film deposition,

both of these problems are obviated. The slide with the indium smears appears as shown in Figure 3(a).

A fairly thick aluminum base layer is next vacuum evaporated onto the substrate. The aluminum is evaporated from a filament of 0.075 inch diameter tungsten wire on which bent pieces of aluminum wire have been hung. An appropriate mask is placed close to the substrate and protects most of it from the aluminum. The result is a base layer in the shape shown in Figure 3(b). All evaporations are done at a pressure of 5×10^{-5} millimeters of mercury or less. Evaporation is continued until the tungsten filament can no longer be seen through the aluminum deposited on the substrate. Later measurements of the resistance of such films show that they are approximately 400 to 500 Angstroms thick.

The critical step in the preparation of a specimen is the oxidation of the aluminum base layer to produce the barrier layer. Previously, in this laboratory, oxidation of the aluminum has been achieved by letting ordinary air, or on some occasions air passed over water, into contact with the specimen. Using this method, the time required to oxidize a good specimen varies from a few minutes to as long as 24 hours depending on the weather, in particular, on the relative humidity. Furthermore, specimens made in this way are unstable ~~as~~ at room temperature, with junction

FIGURE 3

Schematic showing the various stages of specimen preparation.

(a)

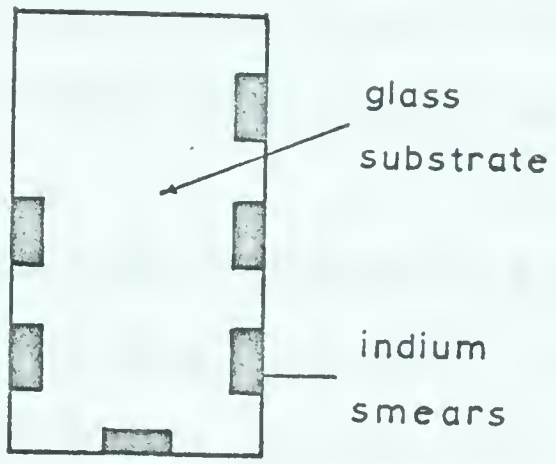
glass
substrate
indium
smears

(b)

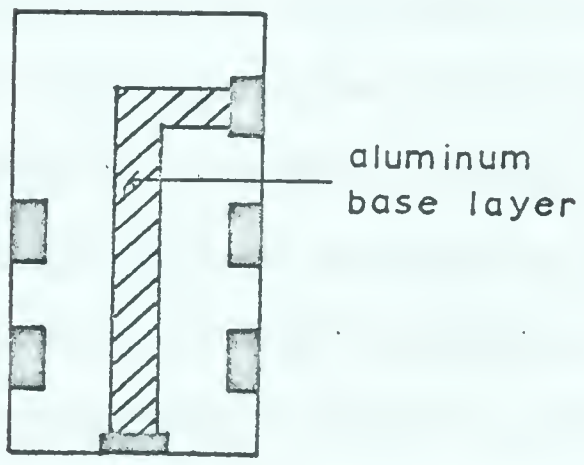
aluminum
base layer

(c)

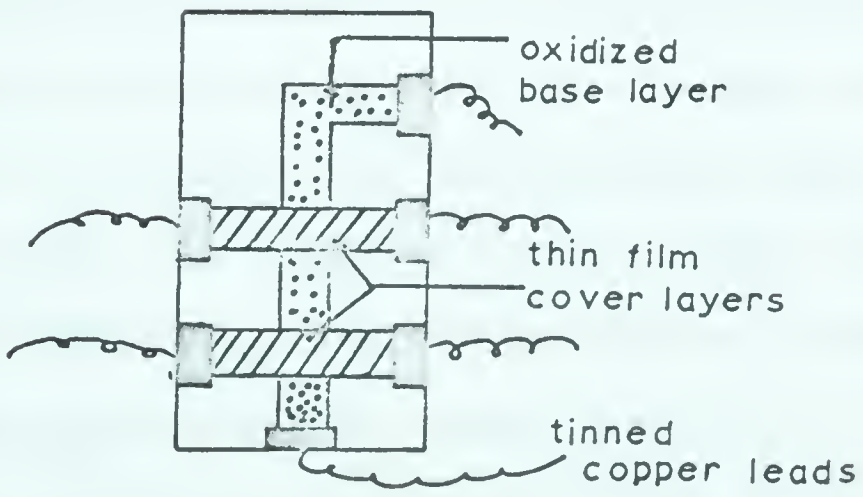
oxidized
base layer
thin film
cover layers
tinned
copper leads

resistances which increase quite rapidly after they are prepared. To stop this, the substrate must be mounted in the specimen chamber and immersed in liquid air as quickly as possible.

The present specimens were oxidized in a furnace with the temperature gradually rising from 230°C. at the beginning of the process to 350°C. at the end. With this method, a typical oxidation time for a junction of between 100 and 400 ohms resistance is one and one half minutes. Two minutes gives a thick barrier layer with a resistance of many megohms, while a one minute oxidation time almost invariably yields a barrier with metallic bridges through it. One obvious advantage of oxidizing in a furnace is that the weather dependence is removed. Another important feature of this method of oxidation is that it seems to bake the oxide layer, thus giving specimens which are quite stable at room temperature. These specimens can be put in the specimen chamber and mounted in the cryostat immediately without the junction resistance increasing to unusable levels.

The thickness of the barrier layers has been estimated from measurements of junction and capacitance, made with the capacitance bridge described by Rogers (1964). These measurements are unreliable except when they are made on specimens in which both aluminum layers are fairly thick, and hence of low resistance. Since the bridge allows only

a two terminal measurement to be made, the resistance of the metallic film, which is appreciable in some of the specimens, is included in the measurement. From the reliable measurements, it is estimated that the oxide barrier thickness produced in one and one half minutes in the furnace is approximately 20 Angstrom units.

It may be noticed that the oxidation temperatures are well above the melting point (140°C.) of the indium smears. During oxidation the indium does melt, but its surface tension is sufficiently great to keep the indium from flowing. Thus it merely melts during oxidation, and solidifies in the original position when it is taken out of the furnace. Better contacts are obtained between the indium and the aluminum of the cover layer if the indium is scraped to remove any possible oxide after the oxidation process.

The next step is to deposit the upper or cover layer, which in the present experiments is the thin film. For this layer, the thickness of the film must be measured, and, in order to exert satisfactory control over the thickness, it must be measured continuously as the film is deposited. This is done simply by monitoring the resistance of the film during deposition. The thickness can then be calculated from the resistance.

Leads from the resistance monitor are attached to

the indium contacts for the cross strips that form the cover layers. The thin films are then evaporated while the resistance is monitored continuously and displayed on a chart recorder. When the resistance is reached that corresponds to the desired thickness, deposition is stopped. Specimens can be prepared in this way, either with a single cross strip or a double one, such as the completed specimen shown in Figure 3(c) with all leads attached. The leads are bare copper wire, tinned with 50-50 tin-lead solder so that at the temperatures of the experiments ($\sim 1^\circ K$), the leads will be superconducting.

As soon as the cover layers are deposited, the resistance of the junction is measured using a four terminal connection and a vacuum tube voltmeter. A good junction has a resistance of approximately 100 to 400 ohms. Resistances of less than 100 ohms generally signify a very thin barrier which is likely to rupture at low temperatures. Resistances larger than 400 to 500 ohms at room temperature will generally rise to unusable values at temperatures near $1^\circ K$.

When a junction with a suitable resistance is obtained its room temperature I-V characteristic is displayed on an oscilloscope. The criterion for the existence of tunneling is that this characteristic be non-linear. Figure 4 shows two examples of this non-linearity. Both photographs are

FIGURE 4

Current-voltage characteristic of a tunnel junction at (a) 300°K, and (b) 80°K. The non-linearity in the curve is evidence that there is tunneling through the barrier layer.

(a)

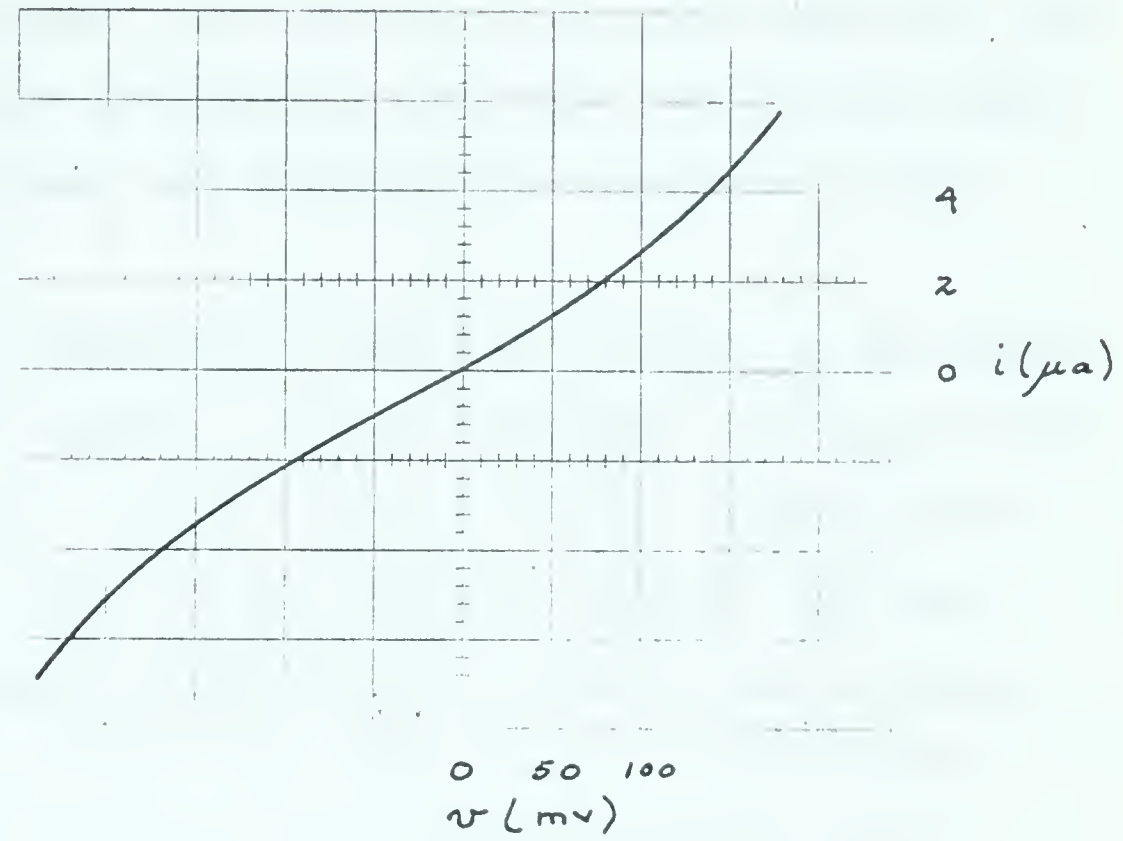

(b)

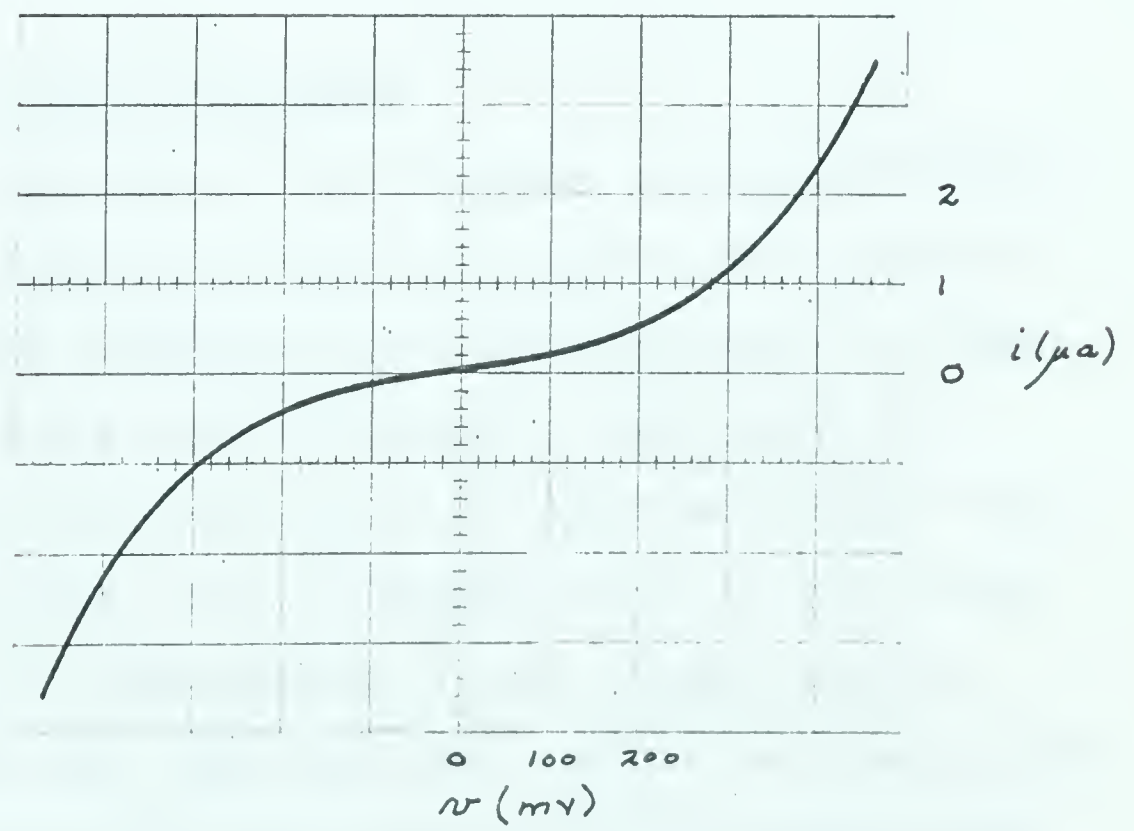

from the same specimen, the first at room temperature and the other at 80°K. These photographs also show the greater dominance of tunneling over other conduction mechanisms at the lower temperature.

If the tunnel junction is found to be good, it is mounted in the specimen chamber, and this assembly is then mounted in the He^3 cryostat. Figure 5 shows a sketch, approximately double the actual size, of the specimen chamber. The pumping tube is provided so that once the specimen is in place, the chamber can be filled with helium gas at atmospheric pressure and then sealed off. At 1°K this helium forms a thin superfluid film over the glass substrate and thus provides thermal contact between the tunnel junction and the base of the specimen chamber.

B. Measurement of Film Resistance

As noted in section A, the thickness of the thin films is controlled by monitoring their resistance during deposition. The circuitry employed to do this monitoring is shown in Figure 6. The largest RMS voltage the oscillator can give is 20 volts. With this input, the maximum voltage which can be applied across a film is approximately 5 millivolts; thus a current of 50 microamperes is the largest passed through a 100 ohm film. The amplifier and the oscillator were both tuned to 1 kilocycle per second. The A.C. signal from

FIGURE 5

Schematic showing the method of specimen mounting and the specimen chamber. This drawing is approximately two times life size.

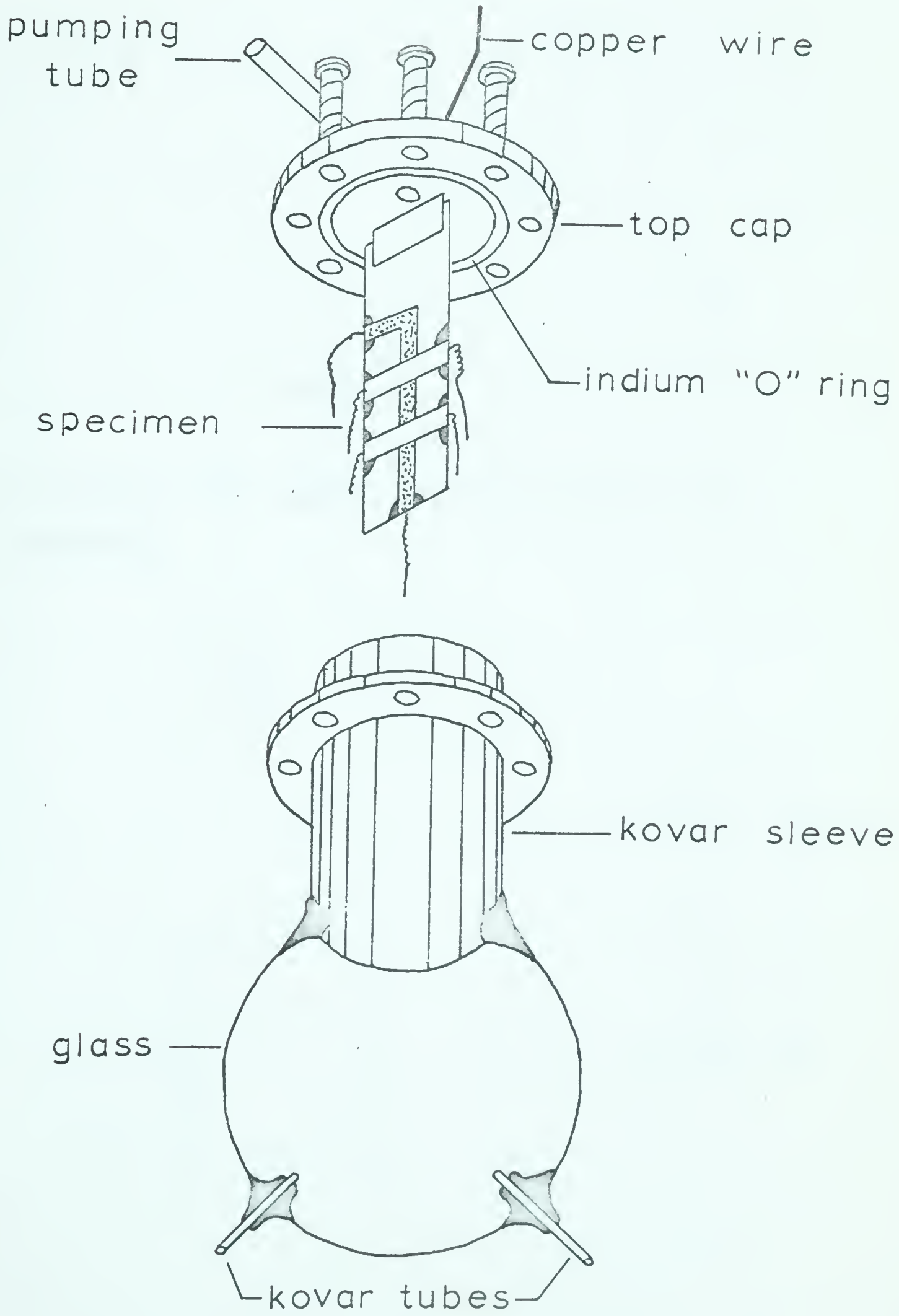
pumping tube
copper wire
top cap
indium "O" ring
specimen
kovar sleeve
glass
kovar tubes

FIGURE 6

Circuit diagram of the apparatus used to monitor the film resistance.

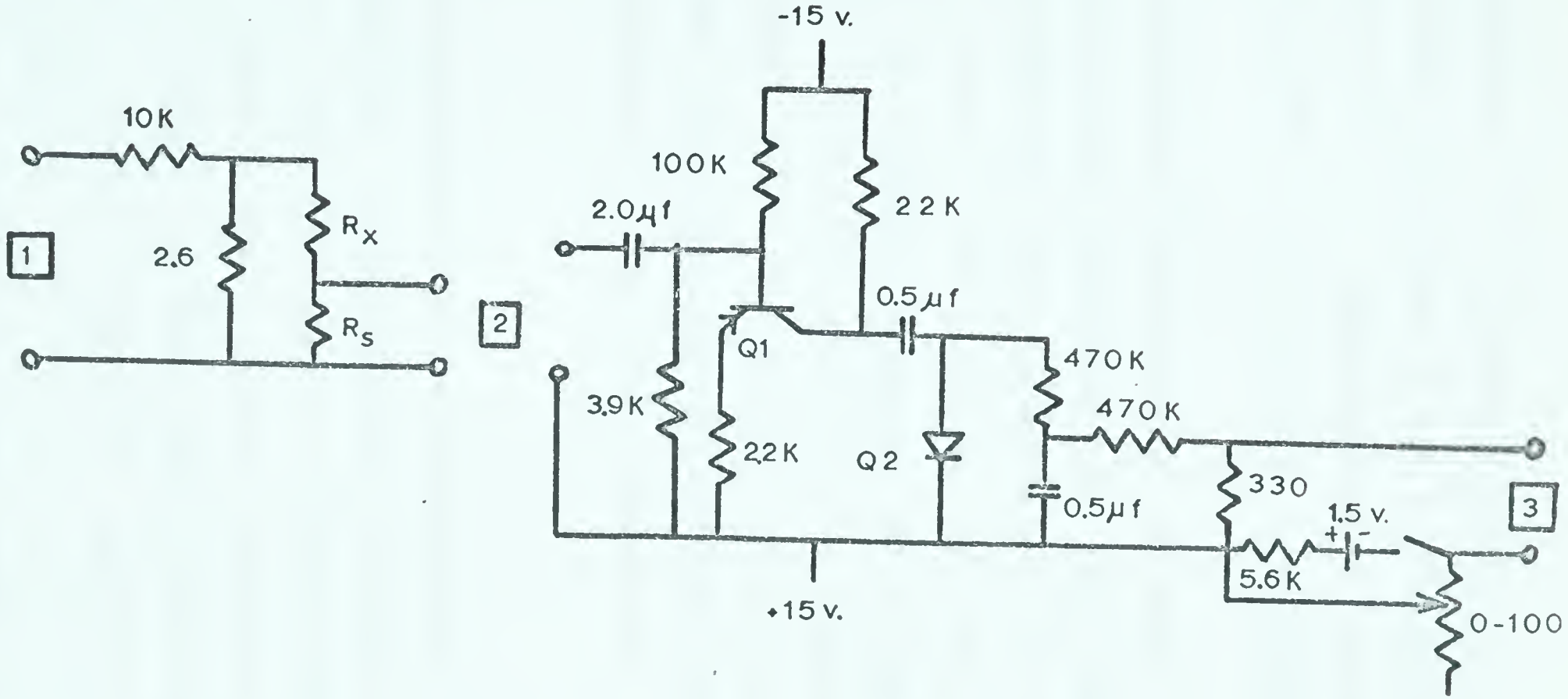

1 HP 200CD Oscillator

2 GR 1232A Tuned Amplifier

3 L-N Chart Recorder

Q1 - 2N1305

Q2 - 1N109

the tuned amplifier and transistor amplifier is rectified by the diode circuit and applied to the chart recorder. The ripple remaining in the d-c signal applied to the chart recorder, which shows as noise on the recorder, is approximately 0.05 millivolts.

Before each thin film deposition the chart is calibrated using a standard resistance box. Then, during the evaporation, deposition can be stopped when the desired film resistance is reached. With the final film resistance recorded on the chart, the standard resistance box is again employed to determine the exact film resistance by comparison. This comparison enables us to determine the film resistances to within $\pm$ 2 ohms. The calculation of the film thickness from the film resistance is discussed in Chapter III.

C. Cryostat

Since the specimens used in the experiments are made of aluminum, which has a superconducting transition temperature of 1.2°K, it is necessary to have a cryostat which will go below 1°K, in order to ensure that the observations are made on a specimen in which the energy gap is fully developed. For this reason, a helium three (He^3) cryostat is used for all the experiments.

Figure 7 is a diagram of the experimental chamber of the cryostat, which consists essentially of a He^3 stage inside a

FIGURE 7

Schematic of the experimental chamber of the He^3 cryostat.

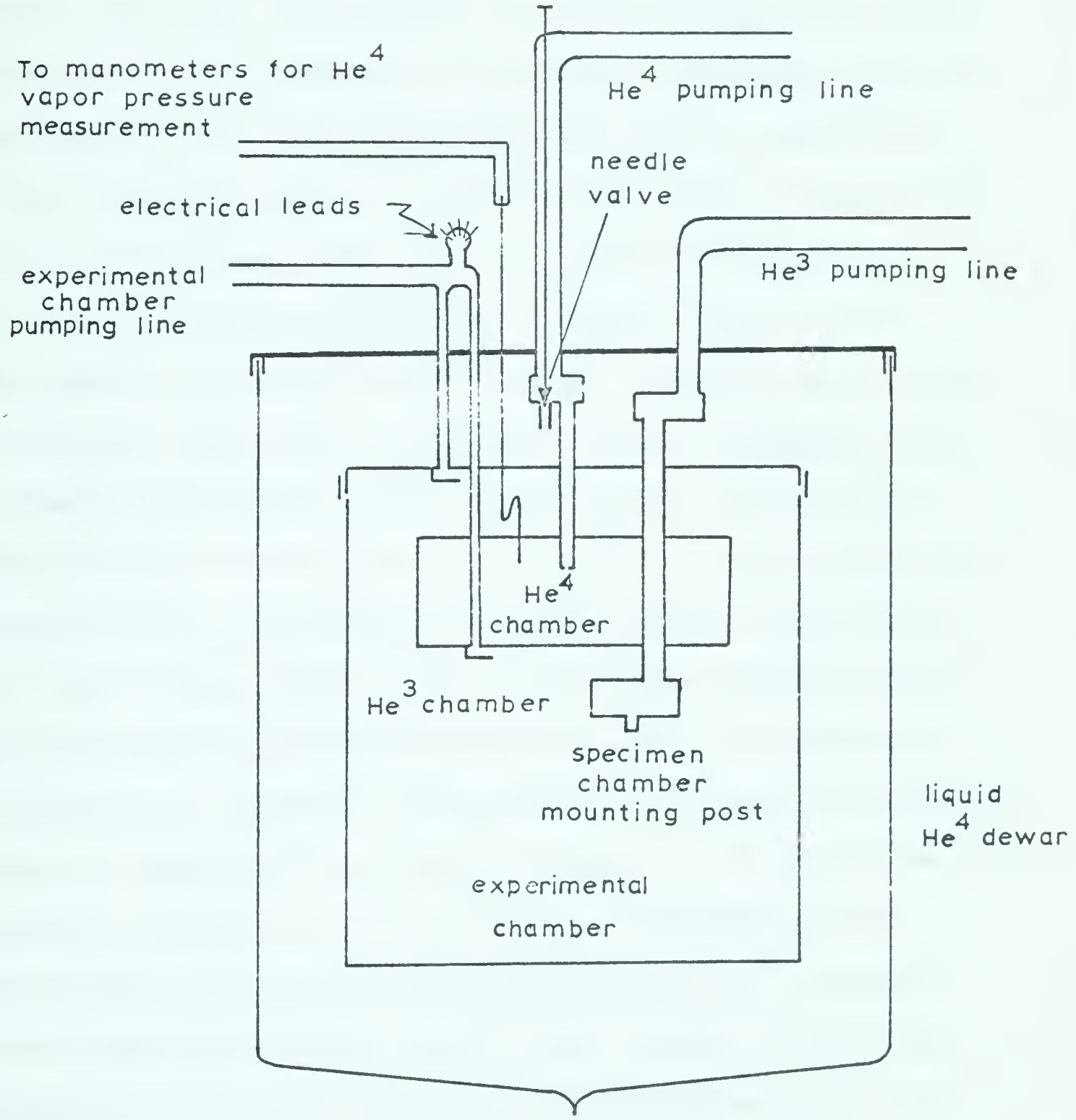
To manometers for He^4 vapor pressure measurement
He^4 pumping line
needle valve
electrical leads
He^3 pumping line
experimental chamber pumping line
He^4 chamber
He^3 chamber
specimen chamber mounting post
liquid He^4 dewar
experimental chamber

He^4 cryostat. The temperature of the He^4 chamber is obtained from oil and mercury manometers that measure the He^4 vapor pressure, while the temperature of the He^3 chamber is determined with a 35 ohm germanium resistance thermometer mounted on the chamber. The specimen holder is held in place by a 0.040 inch diameter copper rod which fits into a hole in the bottom of the He^3 can. The joint is soldered with Wood's metal which is applied liberally in order to get a good thermal contact between the He^3 can and the specimen chamber. The electrical leads are 0.0025 inch diameter manganin wire.

Between experiments the He^3 used by the cryostat is stored in a tank holding one liter of He^3 at room temperature and pressure. The entire He^3 system is closed, and must be free of even "superleaks", which could allow superfluid He^4 to enter the system and contaminate the He^3. In operation, the experimental chamber is precooled with liquid air and then immersed in liquid He^4 as shown in Figure 7. At this time the experimental chamber is filled with He^4 exchange gas to hasten thermal equilibrium while the He^3 and He^4 chambers are evacuated. The exchange gas is next pumped out of the experimental chamber to a pressure of approximately 2×10^{-6} millimeters of mercury. This generally takes about six hours, after which time the low temperature end of the cryostat is at a temperature of about 4°K. When the exchange gas has been pumped out, liquid He^4 is allowed to enter the He^4 chamber

through the needle valve, which is then closed. Pumping on this chamber reduces its temperature to 1.2 or 1.3°K. When this temperature is reached, He^3 gas from the storage can is admitted to the He^3 chamber. As it passes down the tube through the He^4 can, the He^3 is liquified. The He^4 vapor pressure rises as the He^3 liquifies and then settles back to its previous value as the heat of vaporization is removed. The He^3 can is connected to the pump until all the He^3 has been pumped back into storage, at which time another cycle begins as the He^3 is recondensed. Temperatures as low as 0.33°K have been achieved while pumping on the He^3. However, a big disadvantage of this "single-shot" method of operation is that temperatures between 0.33 and 1.2°K can be obtained only by applying heat to the experimental chamber. This heat accelerates the boiling of the He^3 with the result that a "shot" of He^3 (one liter at NTP) is good for approximately two minutes operation at temperatures of 0.80°K and above.

D. Measurement of the I-V Characteristics

The current-voltage characteristics of the tunnel junctions are measured using a modification of the curve tracer described by Rogers, Adler and Woods (1964). Since only the I-V characteristic and not the dynamic conductance is needed, the full circuit is not employed. However, the peculiar grounding arrangement needed to reduce the a-c pickup made it more

convenient to modify the existing circuitry than to use something simpler. The actual circuit used is shown in Figure 8.

The two outputs from the curve tracer are fed into an X-Y oscilloscope for display. The manual sweep built into the power supply is used to trace out the characteristic. The galvanometer amplifier is used as a preamplifier, ahead of the oscilloscope, on either the current or voltage output depending on the data desired. For energy gap and thermometry measurements, where the negative resistance region is most important, it is used on the current (vertical) output, but for the data on energy gap smearing, it is used on the voltage (horizontal) output.

Using an oscilloscope camera, and negative film, photographs were taken of the I-V characteristics. The photographs were then enlarged and traced onto graph paper that had been prepared to fit the actual oscilloscope calibration, not simply the reticule on the oscilloscope face. All measurements were then made from the graphs of the I-V characteristics.

FIGURE 8

Circuit diagram of modified curve tracer used to obtain current-voltage characteristics.

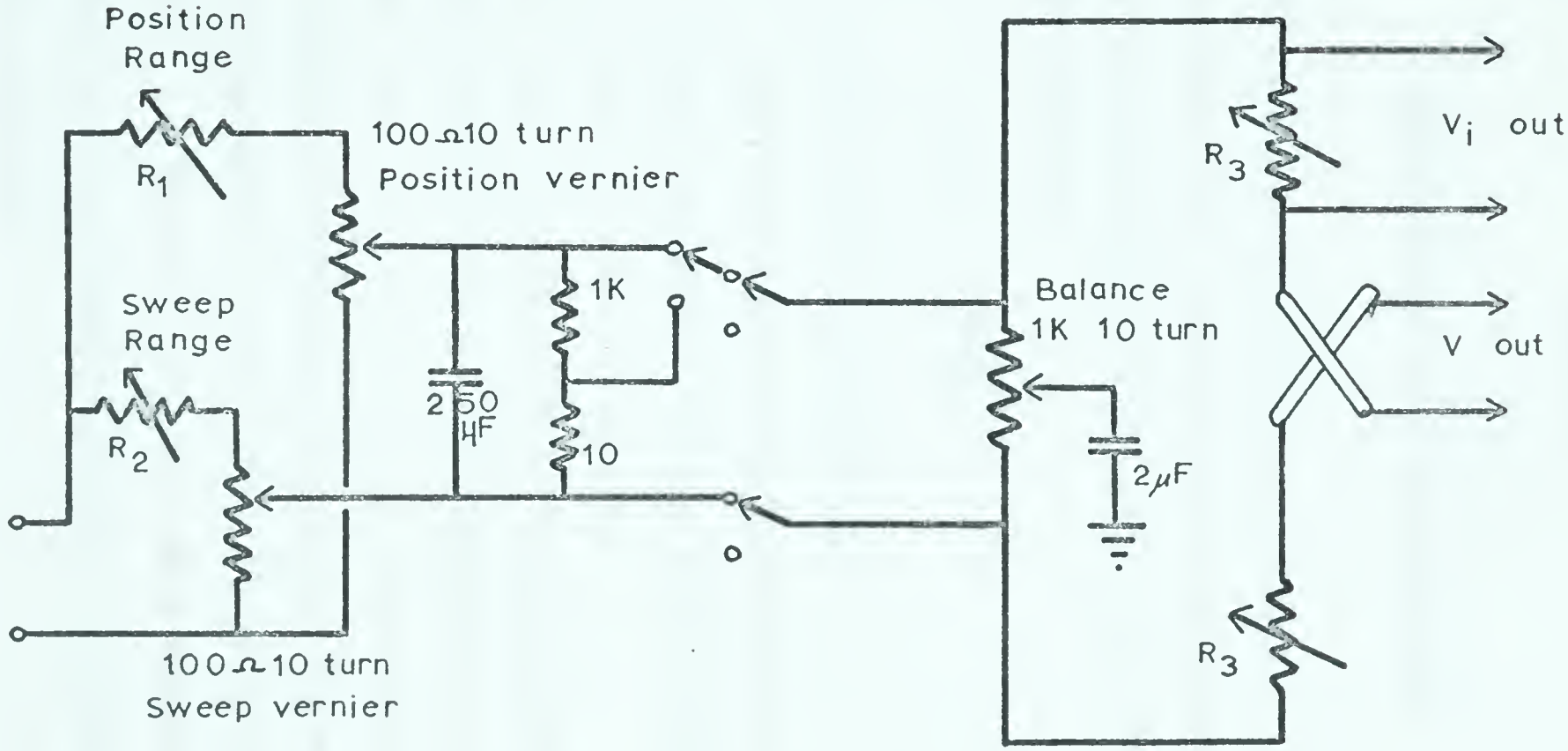

R_1, R_2, and R_3 may be adjusted stepwise to the following values:

R_1 = 0, 470

R_2 = 0, 390, 1.5K, 4.7K, 15K, 47K, 150K, 470K.

R_3 = 10, 100, 1K, 10K, 100K (1%).

CHAPTER III

CALCULATION OF FILM THICKNESS

As mentioned before, it is necessary to calculate the film thicknesses from the resistance measurements and the known lateral dimensions of the film. This can be done using the standard formula

$$R = \frac{\rho L}{w t} \quad , \qquad (1)$$

where R is the film resistance,

ρ is the resistivity of aluminum,

L is the length of the film, (0.86 centimeters),

t is the film thickness,

and w is the film width (0.13 centimeters).

However, difficulties arise because the resistivity of the material in a thin film is not the same as the resisticity of a bulk sample of the same material. The reason for the change in resistivity is that when the film thickness is small enough, collisions with the film surfaces rather than lattice vibrations or impurities may determine the mean free path of the electrons.

We can calculate the electronic mean free path (λ_o) in bulk aluminum using the formula

$$\lambda_o = \frac{2 m v}{\rho_o N e^2} \qquad (2)$$

where λ_o is the electron mean free path in bulk material at room temperature,

ρ_o is the bulk value of resistivity at room temperature, (2.82×10^{-6} ohm-cms. for aluminum),

N is the number of electrons per cubic centimeter, (2×10^{23} electrons per cc., assuming three free electrons per atom of aluminum),

and e,m,v are the electronic charge, mass, and velocity (at the Fermi surface).

The electronic velocity is obtained from the quantum mechanical expression

$$\frac{1}{2} m v^2 = \frac{h^2}{2m} \left[\frac{3N}{8\pi}\right]^{2/3} , \qquad (3)$$

which gives a value of $v = 2.1 \times 10^8$ cm./second. From equation (2), the electronic mean free path in bulk aluminum at room temperature is 133 Angstrom units. Since the thin films used in the experiments are less than 100 A. thick, we must know the variation of resistivity of aluminum with film thickness in order to calculate our film thicknesses.

The resistivity of a thin film was first calculated by J.J. Thomson (1898) who introduced the idea of limitation of the electronic mean free path by the film boundaries. Lovell

(1936) improved upon Thomson's result by noting that for film thicknesses much thinner than the electronic mean free path, all electron free paths may be considered as either beginning or ending on a film surface. He further assumed all electron-surface collisions to be perfectly inelastic, with no correlation between the directions of incidence and reflection in such a collision. With these assumptions, Lovell calculated, by the usual kinetic theory method, the resistivity of a film of thickness t to be

$$\rho = \frac{2mv}{Ne^2} \frac{1}{t\left[1 + \log \lambda_0/t\right]} \quad . \tag{4}$$

Lovell found this result to be in fairly good agreement with experiment for thicknesses greater than 25 A., but below 25 A. his experimental resistivities were even larger than those predicted by his calculations. Using equations (1) and (4), the resistance of one of our films of thickness t is given by

$$R = \frac{L}{w} \frac{2mv}{Ne^2} \frac{1}{t^2\left[1 + \log \lambda_0/t\right]} \quad . \tag{5}$$

This function is shown in the graph of Figure 9.

Using the same assumptions made by Lovell, with a different but still approximate approach, Dingle (1949) calculated the resistivity of a thin film to be

$$\rho/\rho_0 = 1/\left\{k - \tfrac{3}{4}k^2\left(\ln \tfrac{1}{k} + 2.2\right)\right\} \quad , \tag{6}$$

FIGURE 9

Graph showing variation of film resistance with thickness according to Lovell, Dingle, and Fuchs.

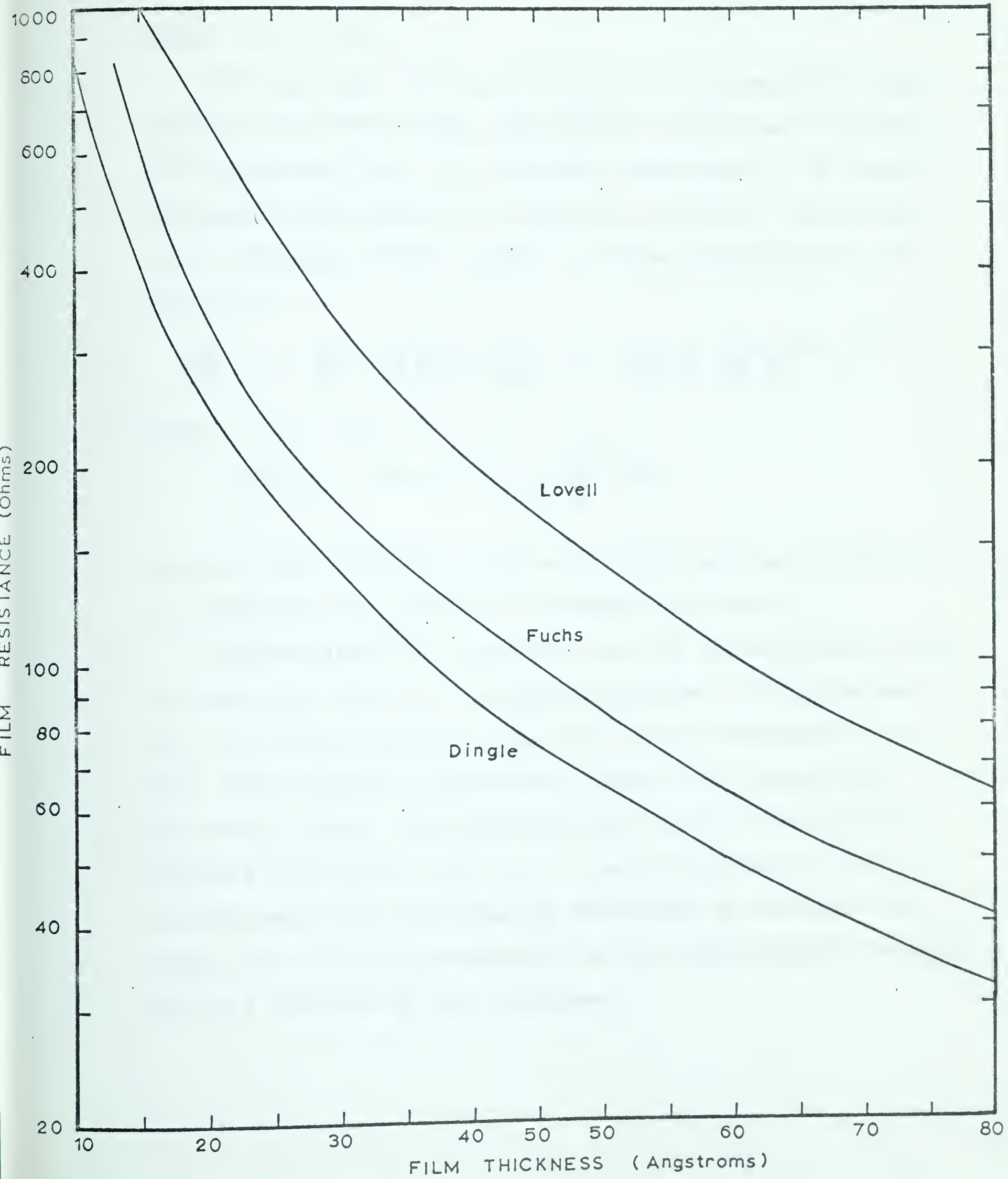
1000
800
600
400
200
100
80
60
40
20
FILM RESISTANCE (Ohms)
Lovell
Fuchs
Dingle
10
20
30
40
50
50
60
70
80
FILM THICKNESS (Angstroms)

where $k = t/\lambda_o$.

The only exact calculation of thin film resistivity has been done by Fuchs (1939), who solved the Boltzmann equation with appropriate thin film boundary conditions. If we introduce again the assumption of perfectly inelastic collisions at the boundary, Fuchs' result, in terms of conductivity σ , reduces to

$$\frac{\sigma}{\sigma_o} = 1 + \frac{3}{4}\left(K - \frac{K^3}{12}\right)B(K) - \frac{3}{8K}\left(1 - e^{-K}\right) - \left(\frac{5}{8} + \frac{K}{16} - \frac{K^2}{16}\right)e^{-K} , \quad (7)$$

where $K = t/\lambda_o$

$$B(x) = -Ei(-x) = \int_x^\infty \frac{e^{-\xi}}{\xi}\, d\xi \quad .$$

Figure 9 also shows the results for film resistance based on the resistivities calculated by Dingle and Fuchs.

Unfortunately, an expression for the increase in resistivity in thin films which is in complete agreement with experiment has not yet been devised. Hence the exact thickness of our thin films cannot be determined. However, the expressions by Lovell, Dingle, and Fuchs do give a means of calculating relative thicknesses which is the major requirement in the present work. This knowledge is sufficient to determine the shape, and possible periodicity, of the superconducting energy gap as a function of film thickness.

CHAPTER IV

ENERGY GAP MEASUREMENTS

A. Shape Resonance Theory

The chief purpose of the present experiments is to check experimentally the theoretical prediction by Blatt and Thompson (1963 a,b) of "shape resonances" in the energy gap as a function of film thickness. Their result comes from the application of boundary conditions to the solution of the basic equations for a superconductor. Details of the theory may be found in the articles cited above, or in "Theory of Superconductivity" by J.M. Blatt.

The result of the above calculations is the energy gap equation

$$C_n = \hbar\omega_c \Big/ \sinh\left[\frac{Ka}{\nu + \gamma_2}\right] \quad \text{for} \quad n \leq \nu$$
$$= 0 \quad \text{for} \quad n > \nu \quad , \tag{1}$$

where ν, n are integers,

$K = k_F/\pi\rho$,

a is the film thickness,

ρ is a non-dimensional coupling parameter,

and k_F is the Fermi momentum.

ν is an integer which increases by one at each resonance in the direction of increasing slab thickness. Hence, it

may be referred to as a "resonance number". For a particular value of ν, the energy gap equation (1) is valid for film thickness in the range $a_\nu + \epsilon(a) < a < a_{\nu+1} - \epsilon(a)$, where $\epsilon(a)$ is a measure of the width of the resonance regions ($\epsilon(a) < 1$ Å), and a_ν is given by

$$a_\nu^3 = \frac{\pi V}{2N}\left\{\nu^3 - \frac{1}{3}\nu\left(\nu+\tfrac{1}{2}\right)(\nu+1)\right\}. \qquad (2)$$

From the conditions on the energy gap equation, it can be seen that a new value of the integer n begins to contribute at each resonance. For example, up to the first resonance, the only C_n which is not zero is C_1. Between the first and second resonances, C_1 and C_2 are non-zero. Theoretically, the integer n is the wave vector component in the same direction as the slab thickness. For example, in a slab of thickness a in the X direction and infinite extent in the Y and Z directions, n is the X component of the wave vector.

We can also calculate the peak and trough resonance values of C_n for a given resonance number. Respectively, they are given by

$$C_{P,\nu} = \frac{\hbar\omega_c}{\sinh\left\{\frac{k_F a_\nu}{\pi p(\nu+1/2)}\right\}}, \qquad (3)$$

and

$$C_{T,\nu} = \frac{\hbar\omega_c}{\sinh\left\{\frac{k_F a_\nu}{\pi p(\nu-1/2)}\right\}}. \qquad (4)$$

Figure 10 shows the graph of the energy gap function C_n

FIGURE 10

Graph of the energy gap function C_n. This graph shows C_n plotted against film thickness, t.

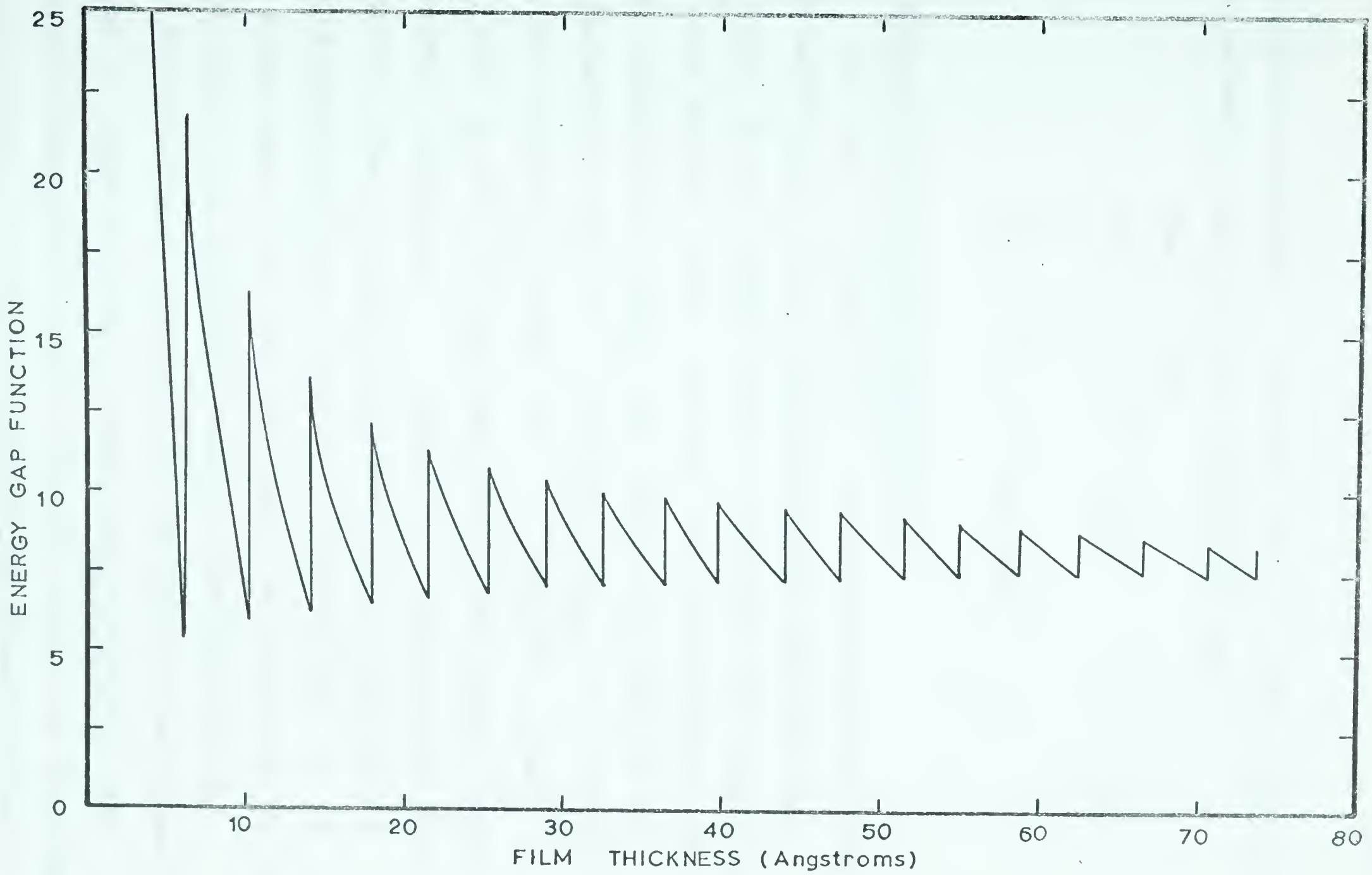
ENERGY GAP FUNCTION
0
5
10
15
20
25
10
20
30
40
50
60
70
80
FILM THICKNESS (Angstroms)

plotted as a function of thickness from the above equations. The parameters used in these calculations are

$$\begin{aligned} \hbar\omega_c &= 100^\circ K \\ N/V &= 2 \times 10^{22} \ /cm.^3 \\ \rho &= 0.3 \\ k_F &= 8.2 \times 10^7 \text{ cms./sec.} \end{aligned} \qquad (5)$$

B. Results of Energy Gap Measurements

When the I-V characteristic of a tunnel junction with both metal layers in the superconducting state has been obtained, it is a simple matter to calculate the energy gap for each metallic layer. The bases for the calculation has been illustrated in Figure 1(c), Page 2. The cusp in the characteristic occurs at an applied voltage of $V = \frac{\Delta_1 - \Delta_2}{e}$ and the current jump occurs at $V = \frac{\Delta_1 + \Delta_2}{e}$, where Δ_1 and Δ_2 are the energy gaps in the two layers. Figure 11 shows a photograph of a typical I-V characteristic and Figure 12 shows the graph obtained from it, along with a sample calculation of Δ_1 and Δ_2. In this case, Δ_1 is the energy gap in the thin film, while Δ_2 is the gap in the thick film, which presumably behaves like bulk material.

The experiments reported here consisted of measurements of the I-V characteristic of seven tunnel junctions with different thicknesses of thin film. The results of the energy gap calculations for these specimens are shown in Table I.

FIGURE 11

Photograph of a typical current-voltage characteristic.

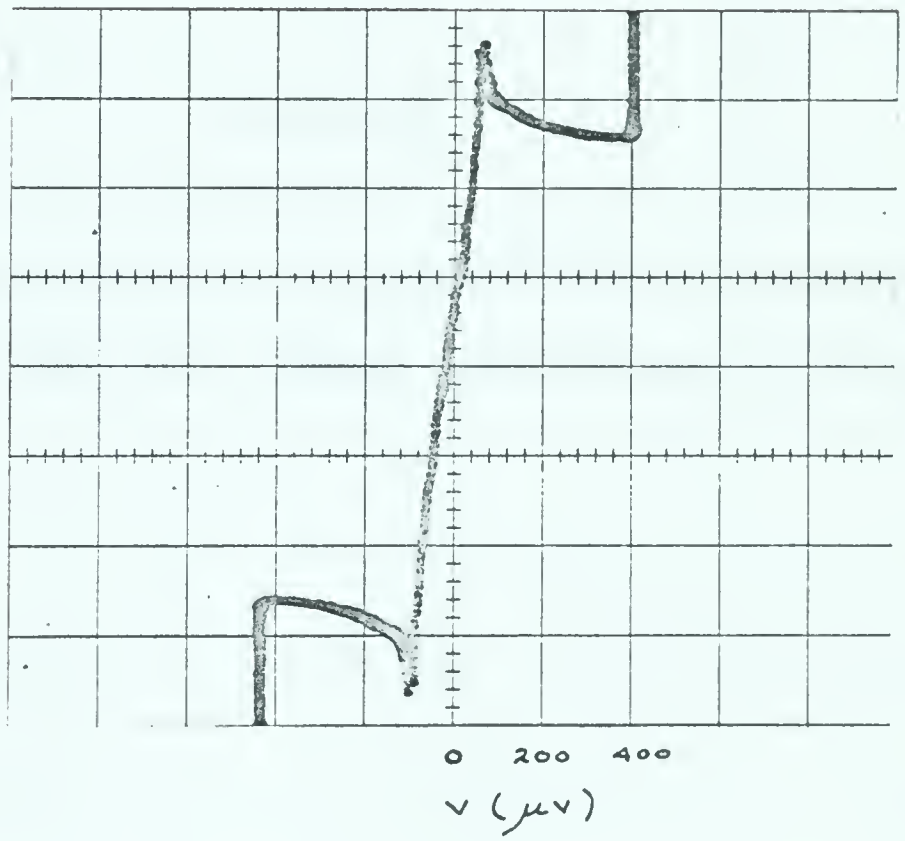
i
(arbitrary
units)
0
200
400
V (μV)

FIGURE 12

Graph of I-V characteristic projected from the photograph of Figure 11. Also shown is a sample calculation of $\triangle_1$ and $\triangle_2$.

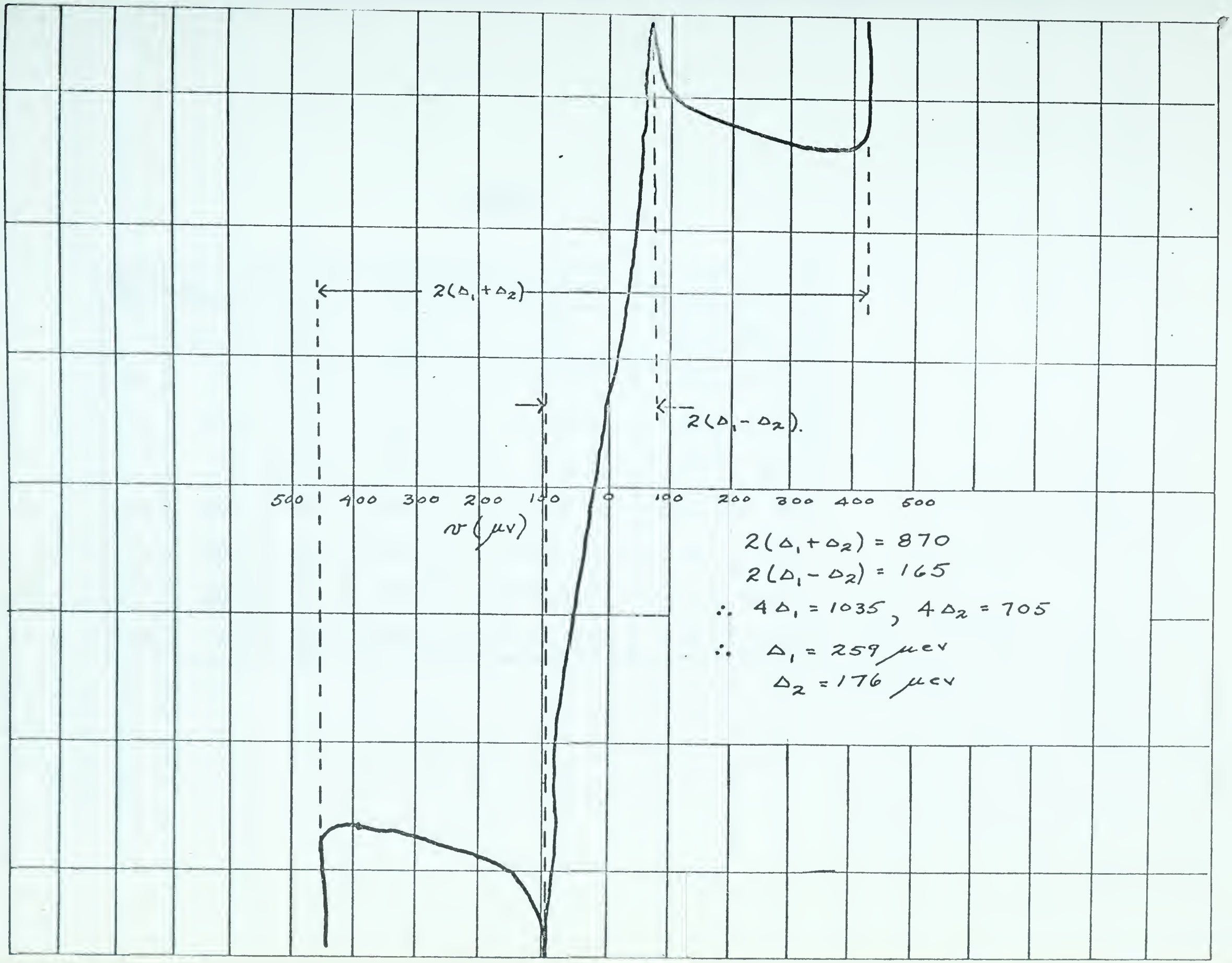

$2(\Delta_1 + \Delta_2) = 870$

$2(\Delta_1 - \Delta_2) = 165$

$\therefore\ 4\Delta_1 = 1035,\ 4\Delta_2 = 705$

$\therefore\ \Delta_1 = 259\ \mu ev$

$\Delta_2 = 176\ \mu ev$

TABLE I

Spec. #	R_{film}	t	$\Delta_1(0)$	$\Delta_2(0)$	T_{c1}	T_{c2}
	Ohms	A.	μev	μev	°K	°K.
1	73	55	265 ± 15	185 ± 15	1.8	1.2
2	141	36	285 ± 20	195 ± 20	1.9	1.3
3	76	53	260 ± 15	190 ± 15	1.7	1.3
5	292	22	310 ± 15	180 ± 15	2.0	1.2
6	180	29	300 ± 15	210 ± 15	2.0	1.4
7.	290	22	320 ± 10	200 ± 10	2.1	1.3
8.	93	47	280 ± 10	170 ± 10	1.8	1.1

This table shows:

1. The resistance of the thin film in each junction.
2. The corresponding thickness of the thin film in each junction. The thicknesses shown are calculated using the expression developed by Fuchs. Since we have only relative thicknesses, this one formula is sufficient. Use of Lovell's or Dingle's expression would not materially alter the results.
3. Superconducting energy gap values for the thick films and the thin films. These values are obtained at a temperature of 0.33°K and can be assumed to equal the value of the gap at 0°K.
4. Transition temperatures for the thin films and the thick films. These transition temperatures are calculated using

$$2\Delta_o = 3.52\, k T_c$$

where $2\Delta_o$ is the full energy gap at at 0°K,

k is the Boltzmann constant,

and T_c is the transition temperature.

The possible error in each particular energy gap value (each photograph) is approximately 10% for the large gaps

(thin film) and 15% for the small ones (thick film). These errors correspond to an uncertainty of 25 microvolts (μv) in the positions of the cusp and current jump. The errors shown in Table I are less than this because in most cases the results from a number of pictures were averaged to get the value shown in the table.

C. Discussion of Energy Gap Results

Figure 13 is a graph showing the experimental variation of the superconducting energy gap with thickness in thin films. Since the usual bulk value of Δ_0 is approximately 0.20 milli-electron volts (mev), these results show fairly definitely that the thin film gap is much larger than the energy gap in bulk material. Insofar as oscillatory behaviour is concerned, it is easy to see that these results bear very little resemblance to the "shape resonance" curve of Figure 10. The dotted lines on the graph represent the peak and trough values of the "shape resonance" curve. Bearing in mind that the possible error in the energy gap points is as much as $\pm$15%, it could be said that the experimental results are not inconsistent with these curves.

If the above is actually the case, it can be explained easily enough. Our films are not perfectly uniform and for a given specimen, the energy gap measured is probably an average over 15 or 20 Angstroms rather than the gap for one

FIGURE 13

Graph of experimental results showing variation of superconducting energy gap with film thickness.

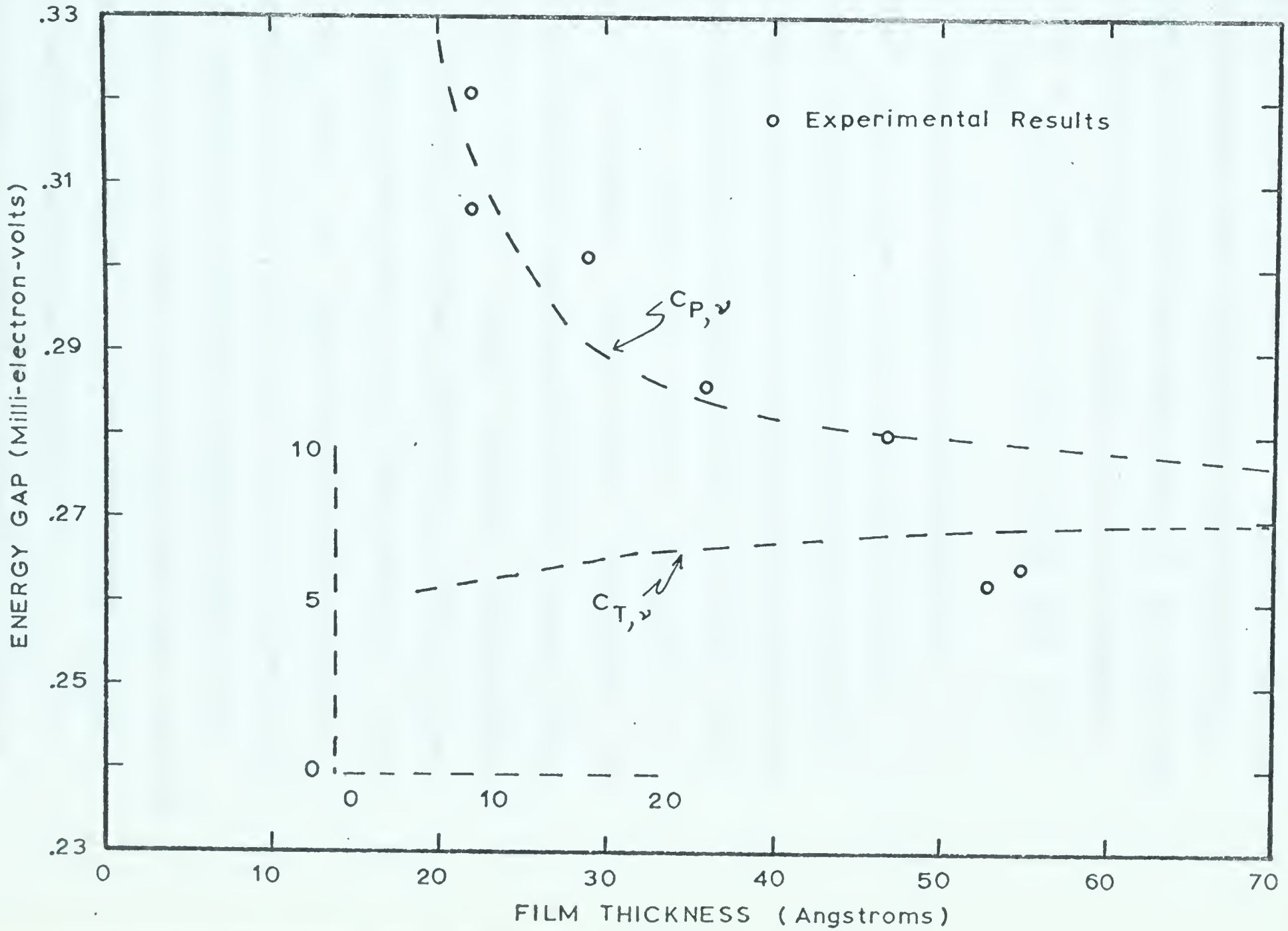
o Experimental Results
$C_{P,\nu}$
$C_{T,\nu}$
ENERGY GAP (Milli-electron-volts)
.33
.31
.29
.27
.25
.23
10
5
0
0
10
20
0
10
20
30
40
50
60
70
FILM THICKNESS (Angstroms)

particular thickness. From the shape resonance curve, such an average should yield a gap larger than the bulk value but less than the resonance peak value. This hypothesis holds good for the points at thicknesses less than 50 A., but the two points for thicker films do not fit. In an averaging process it would be impossible to obtain energy gaps less than the bulk value.

The above results are consistent with Blatt and Thompson in that they do show an increased gap in thin films, but Toxen (1961) has explained an increase in transition temperature (and hence an increased energy gap) on the basis of the variation with thickness of the critical yield stress in thin films. Working with films of the order of 5,000 to 10,000 A. thickness, Toxen found an increase in the superconducting transition temperature for the thinner films. He attributed this effect to strains caused by differential contraction of the film and glass substrate as the specimen is cooled from room temperature to T_c. Other workers (Lock, 1951; Zavaritskii, 1951) have offered additional evidence for this hypothesis. If the rise in T_c due to a volume strain in the film is calculated, the result is much larger than the observed shifts in T_c. Hence, it is concluded that plastic flow takes place in the films, relieving the large thermal stresses which would otherwise be present.

Toxen calculates the variation expected in T_c using a

model in which it is assumed that plastic flow will occur by the motion of dislocations whose ends are pinned at grain boundaries or at the upper and lower surfaces of the film. From this model, the minimum uniaxial stress to cause plastic flow can be calculated and it is found to be of the form

$$P_{min} = C/d \qquad (6)$$

where d is film thickness and C is a constant, depending on the lattice structure of the material involved, its elastic constants, and its orientation with respect to the substrate. Jennings and Swenson (1958) give a relation between hydrostatic pressure and shift in T_c as

$$\delta T_c = -4.36 \times 10^{-5} P_{hyd} + 5.2 \times 10^{-10} P_{hyd}^2 \qquad (7)$$

The effect of the biaxial stress exerted on the films is roughly two-thirds that of a hydrostatic stress of the same magnitude. Hence we expect the variation of T_c with film thickness to be given by a relation of the form

$$\delta T_c = \frac{A}{d} - \frac{B}{d^2} \qquad (8)$$

Figure 14 shows our experimental results in terms of thin film transition temperatures (calculated from $2\Delta_o = 3.52kT_c$). A function of the form $(A/d - B/d^2)$ was calculated by adjusting the constants A and B to give the best fit to the experimental results. The result is the

FIGURE 14

Graph of experimental results in terms of film transition temperatures. The graph shows the variation of these transition temperatures with film thickness. Also shown is the function $T_c = 1.20 + 38/d - 410/d^2$.

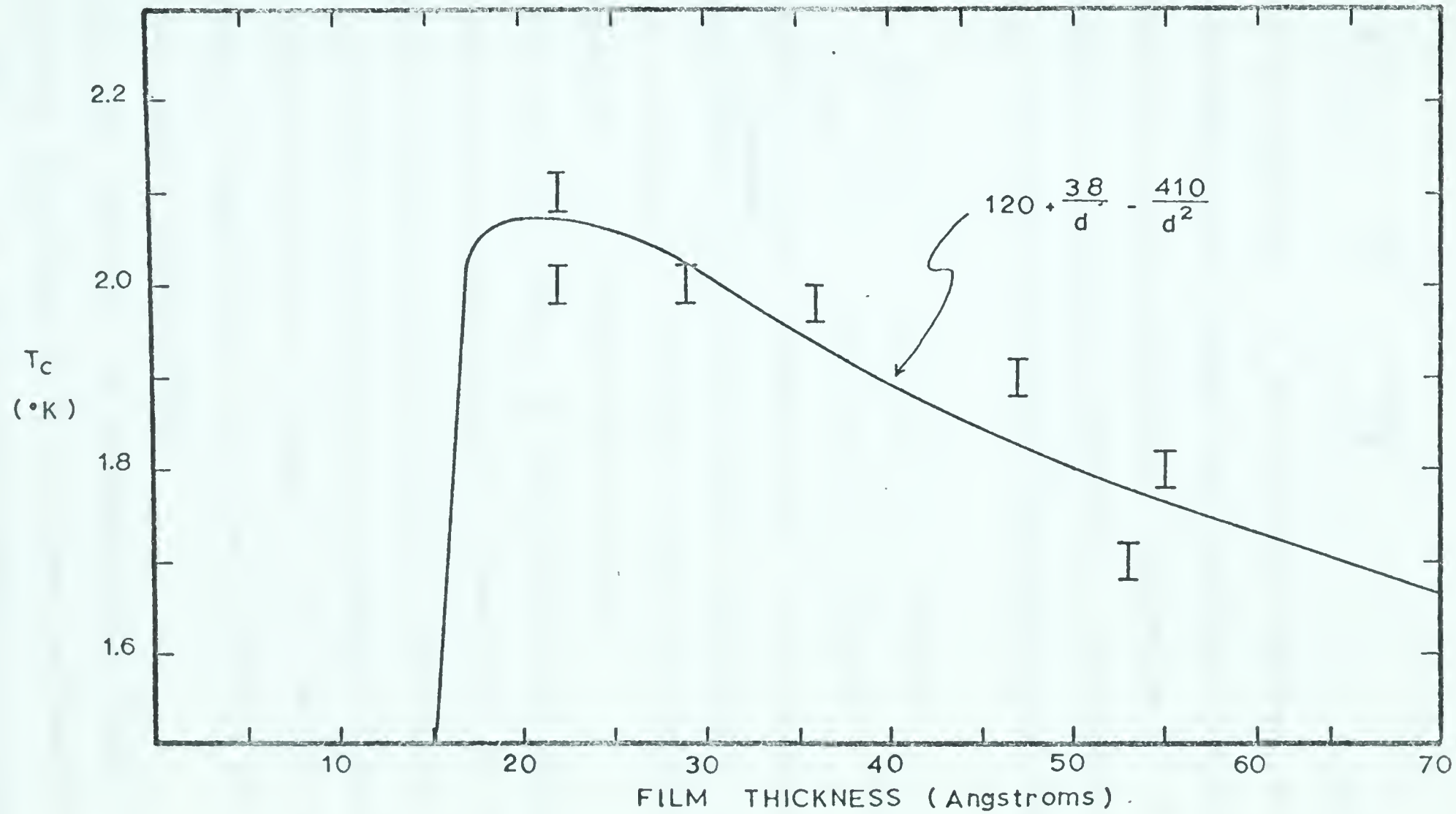
2.2
2.0
1.8
1.6
T_c
(°K)
$120 + \frac{38}{d} - \frac{410}{d^2}$
10
20
30
40
50
60
70
FILM THICKNESS (Angstroms)

expression

$$\delta T_c = \frac{38}{d} - \frac{410}{d^2} \qquad (9)$$

where d is in Angstroms, T_c is in Kelvin degrees, and represents the difference between the transition temperature for bulk material, and the transition temperature for a film of thickness d. Working backwards, we can calculate a value of P_{min} from each of A and B. The results are, respectively,

$$P_{min}\,(A) = 4.35 \times 10^5 / d \text{ atmos}$$
$$P_{min}\,(B) = 4.43 \times 10^5 / d \text{ atmos} \qquad (10)$$

The excellent/of these two answers leads to the conclusion
agreement
that our experimental results are easily explained by Toxen's strain theory, whereas any relation to Blatt and Thompson's "shape resonances" is a tenuous one at best.

P_{min} for our films cannot be calculated from data on aluminum since electron microscopy has shown that our films are composed of randomly-oriented aluminum crystallites. Toxen has calculated the values of the constants A and B for a film of indium obtaining A = 46 and B = 574, which are of the same order of magnitude as the values obtained from our experimental results (A=38, B=410).

One very good check on the agreement with Toxen's theory is given by very thin films (< 20 A) since the function $(38/d - 410/d^2)$ begins to vary quite rapidly at a thickness

of approximately 18 A. Toxen never ran into this problem since the function is a monotonic one in the range of thicknesses which he investigated. The major problem in investigating the region of rapid variation is that the films involved are only a few atomic layers thick and it becomes very difficult to prepare good tunnel junctions when such "ultra-thin" films are involved. In the attempts made to date, it has been found very difficult to obtain junctions with any degree of conduction by tunneling.

CHAPTER V

USE OF TUNNEL JUNCTIONS AS THERMOMETERS

A, Theory

The attempt to use tunnel junctions as thermometers is based on the fact that for an applied voltage slightly less than $V = \frac{\Delta_1 + \Delta_2}{e}$, the tunnel current is made up entirely of thermally excited electrons. For a particular voltage applied to a given specimen, the variation of the tunnel current with temperature should be due only to the variation in the number of thermally excited electrons. The resultant variation in the tunnel current has been calculated approximately by Rogers (1964) for a symmetric tunnel junction (one in which $\Delta_1 = \Delta_2$). However, since the present experiments deal only with non-symmetric junctions ($\Delta_1 \neq \Delta_2$), Rogers' result must be converted to cover this case.

Figure 15 shows a density of states diagram corresponding to an applied voltage $(\frac{\Delta_1 + \Delta_2}{e})^-$ slightly less than $\frac{\Delta_1 + \Delta_2}{e}$, along with an I-V characteristic illustrating the current at $(\frac{\Delta_1 + \Delta_2}{e})^-$.

An approximate expression for the current i_{ss} for a symmetric junction with both metal layers in the superconducting state can be written

FIGURE 15

Illustration of the use of a tunnel junction as a thermometer.

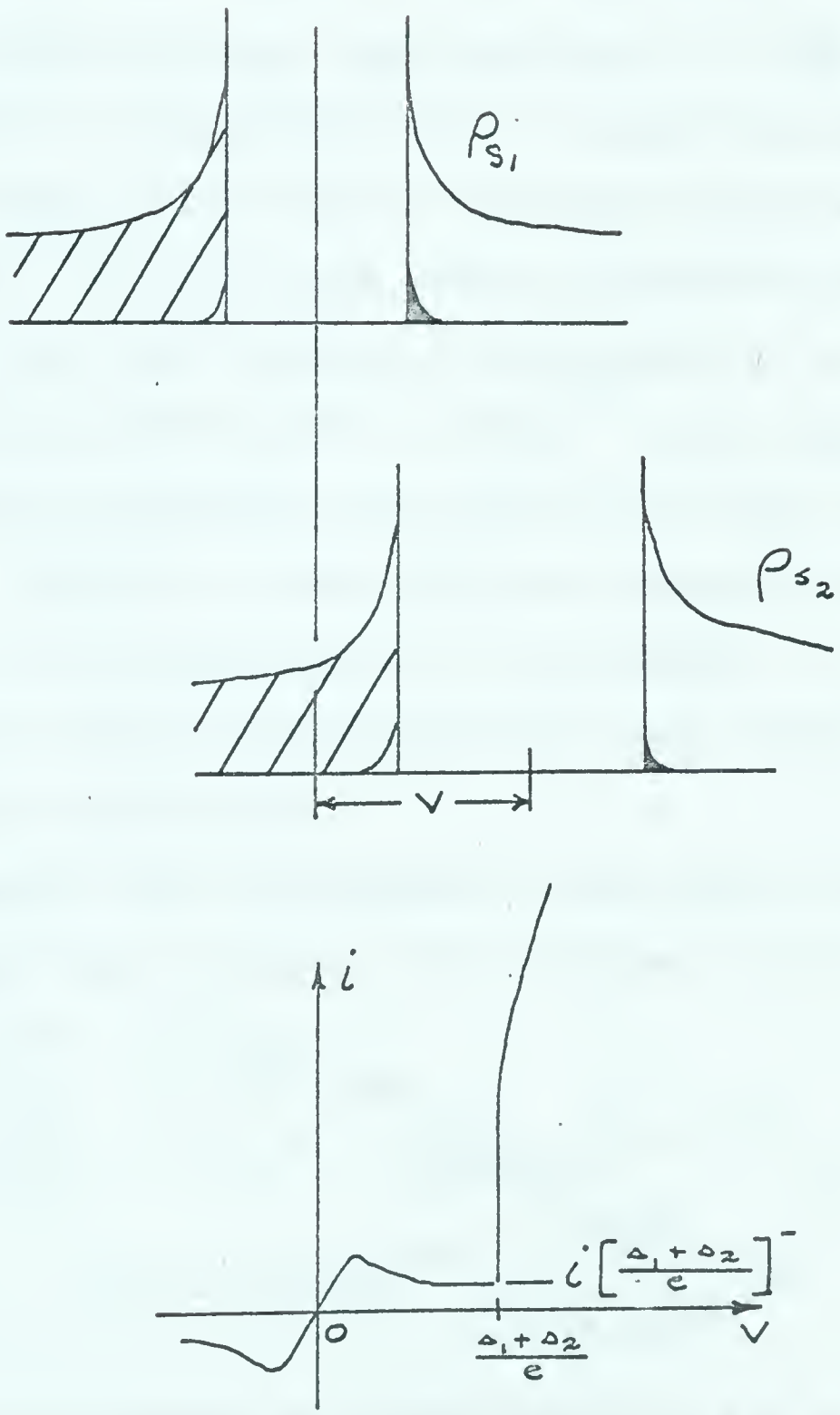
ρ_{s_1}
ρ_{s_2}
V
i
$i\left[\frac{\Delta_1+\Delta_2}{e}\right]^-$
0
$\frac{\Delta_1+\Delta_2}{e}$
V

$$i_{ss}\left[\left(\frac{\Delta_1+\Delta_2}{e}\right)^-\right] = 2C\int_0^\infty e^{-\frac{x+\Delta}{T}}\left(\frac{\Delta}{2x}\right)^{1/2} 1.06\, dx \qquad (1)$$

where C is a constant and $x=E-\Delta$. The first ~~term~~ factor in the integrand is the Fermi function approximation for $\frac{\Delta+x}{T} \gg 1$; the second ~~term~~ factor is the asymptotic form of the BCS function G for $E=\Delta^+$, and the factor 1.06 is the value of $G(2\Delta)$. The factor $\left(1-e^{-2\Delta/T}\right)$ due to the reverse current has been ignored. Even so, the major source of discrepancy in the approximation is due to the factor $(\Delta/2x)^{1/2}$ which departs seriously from the BCS function for values of E close to 0 and close to Δ . However, it does yield an expression which can be integrated. The significance of the variable x is that it represents energy measured from the edge of the energy gap rather than the Fermi level.

If we now convert this expression to the case of the non-symmetric junction shown in Figure 15, and revert to the energy E in place of x, we get

$$i_{ss}\left[\left(\frac{\Delta_1+\Delta_2}{e}\right)^-\right] = 2C\int_0^\infty e^{-E/T}\left(\frac{\Delta_2}{2(E-\Delta_2)}\right)^{1/2} 1.06\, dE \qquad (2)$$

$$= 2.12\, C\,(\Delta_2)^{1/2} e^{-\Delta_2/T}\int_0^\infty \frac{e^{-\frac{(E-\Delta_2)}{T}}}{(E-\Delta_2)^{1/2}}\, dE$$

This integral can be reduced to a gamma function and we can write the normalized current as

$$I = \frac{i_{ss}\left[\left(\frac{\Delta_1+\Delta_2}{e}\right)^-\right]}{i_{nn}\left(\frac{\Delta_1+\Delta_2}{e}\right)} = 1.33\left(\frac{T}{\Delta_2}\right)^{1/2} e^{-\Delta_2/T} \qquad (3)$$

where the value of Δ_2 is understood to be in units of Kelvin degrees.

B. Experimental Results

In order to study the thermometry properties of tunnel junctions, photographs were taken of the I-V characteristics at different temperatures, ranging from 0.33 to 1.1 K. In each case the current at a voltage $\left(\frac{\Delta_1 + \Delta_2}{e}\right)^-$ was measured, along with the energy gaps in the two films. The results thus obtained are shown in Tables II to VIII. From the I-V characteristics of the junctions with both metals in the normal state, the normal state current (i_{nn}) could be found. It was then possible to calculate the normalized current, I, to compare with the theoretical result obtained in Section A.

It was also desired to compare the temperature variation of the energy gap with that given by BCS theory. Hence the values of $\frac{\Delta_2(T)}{\Delta_2(0)}$, $\frac{\Delta_1(T)}{\Delta_1(0)}$, $\frac{T}{T_{c_1}}$, and $\frac{T}{T_{c_2}}$ were calculated. The values of $\Delta_1(0)$ and $\Delta_2(0)$ are simply the results given in Chapter IV for the thin and the thick films respectively. The values of T_{c1} and T_{c2}, the superconducting transition temperatures of the respective films, are calculated using $\Delta_1(0)$, $\Delta_2(0)$ and the formula

$$2\Delta_0 = 3.52\, k T_c$$

The results of the above calculations are shown in Tables II to VIII.

TABLE II

Specimen #1

T	I	$\Delta_1(T)$	$\frac{\Delta_1(T)}{\Delta_1(0)}$	T/T_{c1}	$\Delta_2(T)$	$\frac{\Delta_2(T)}{\Delta_2(0)}$	T/T_{c2}
(°K)	---	μev			μev		
0.40	2.5×10^{-3}	255	0.97	0.23	195	1.05	0.33
0.40	2.5×10^{-3}	265	1.00	0.23	190	1.03	0.33
0.51	8.4×10^{-3}	264	1.00	0.29	178	0.96	0.42
0.51	8.3×10^{-3}	273	1.03	0.29	182	0.98	0.42
0.58	1.5×10^{-2}	262	0.99	0.33	182	0.98	0.48
0.70	2.8×10^{-2}	259	0.98	0.40	176	0.95	0.57
0.80	4.5×10^{-2}	256	0.97	0.46	174	0.94	0.65

TABLE III

Specimen #2

T	I	$\Delta_1(T)$	$\frac{\Delta_1(T)}{\Delta_1(0)}$	$\frac{T}{T_{c_1}}$	$\Delta_2(T)$	$\frac{\Delta_2(T)}{\Delta_2(0)}$	$\frac{T}{T_{c_2}}$
°K	—	μev			μev		
0.33	4.8×10^{-3}	295	1.03	0.17	195	1.00	0.26
0.33	5.8×10^{-3}	285	1.00	0.17	198	1.01	0.26
0.50	3.0×10^{-2}	279	0.98	0.26	191	0.98	0.39
0.69	1.1×10^{-1}	275	0.96	0.36	188	0.96	0.54
0.80	2.0×10^{-1}	268	0.94	0.42	172	0.88	0.62
0.90	2.8×10^{-1}	270	0.94	0.48	165	0.85	0.70

TABLE IV

Specimen #3

T	I	$\Delta_1(T)$	$\frac{\Delta_1(T)}{\Delta_1(0)}$	$\frac{T}{T_{c_1}}$	$\Delta_2(T)$	$\frac{\Delta_2(T)}{\Delta_2(0)}$	$\frac{T}{T_{c_2}}$
°K		μev			μev		
0.33	2.2×10^{-3}	280	1.07	0.19	188	1.00	0.26
0.33	2.4×10^{-3}	256	0.98	0.19	189	1.00	0.26
0.41	7.4×10^{-3}	258	0.98	0.24	188	1.00	0.33
0.50	2.0×10^{-3}	260	0.99	0.29	195	1.03	0.40
0.60	4.1×10^{-2}	260	0.99	0.35	185	0.97	0.48
0.70	7.5×10^{-2}	254	0.97	0.41	176	0.93	0.56

TABLE V

Specimen #5

T	I	$\Delta_1(T)$	$\frac{\Delta_1(T)}{\Delta_2(0)}$	$\frac{T}{T_{c1}}$	$\Delta_2(T)$	$\frac{\Delta_2(T)}{\Delta_2(0)}$	$\frac{T}{T_{c2}}$
°K		μev			μev		
0.33	1.4×10^{-3}	300	0.97	0.16	175	0.97	0.27
0.33	2.1×10^{-3}	316	1.02	0.16	181	1.00	0.27
0.40	1.3×10^{-3}	298	0.96	0.20	182	1.00	0.33
0.50	2.0×10^{-3}	310	1.00	0.25	180	1.00	0.42
0.60	3.4×10^{-3}	310	1.00	0.30	180	1.00	0.50
0.60	3.8×10^{-3}	298	0.96	0.30	180	1.00	0.50

TABLE VI

Specimen #6

T	I	$\Delta_1(T)$	$\frac{\Delta_1(T)}{\Delta_1(0)}$	$\frac{T}{T_{c1}}$	$\Delta_2(T)$	$\frac{\Delta_2(T)}{\Delta_2(0)}$	$\frac{T}{T_{c2}}$
°K		μev			μev		
0.33	5.8×10^{-3}	302	1.01	0.16	212	1.01	0.24
0.33	5.5×10^{-3}	302	1.01	0.16	217	1.03	0.24
0.40	6.7×10^{-3}	299	1.00	0.20	206	0.98	0.29
0.50	9.9×10^{-3}	305	1.02	0.25	215	1.02	0.36
0.60	1.5×10^{-2}	300	1.00	0.30	205	0.98	0.43
0.70	1.7×10^{-2}	300	1.00	0.35	200	0.95	0.50
0.82	2.8×10^{-2}	264	0.88	0.41	216	1.03	0.59

TABLE VII

Specimen #7

T	I	$\Delta_1(T)$	$\frac{\Delta_1(T)}{\Delta_1(0)}$	$\frac{T}{T_{c1}}$	$\Delta_2(T)$	$\frac{\Delta_2(T)}{\Delta_2(0)}$	$\frac{T}{T_{c2}}$
°K		μeV			μeV		
0.33	2.4×10^{-2}	306	0.96	0.16	194	0.96	0.25
0.33	2.0×10^{-2}	324	1.01	0.16	201	1.00	0.25
0.33	1.3×10^{-2}	322	1.00	0.16	205	1.02	0.25
0.40	1.6×10^{-2}	329	1.02	0.19	206	1.02	0.30
0.40	1.5×10^{-2}	310	0.97	0.19	190	0.95	0.30
0.50	2.0×10^{-2}	314	0.98	0.24	199	0.98	0.37
0.71	3.1×10^{-2}	312	0.97	0.33	188	0.93	0.53
0.80	4.5×10^{-2}	304	0.95	0.38	184	0.91	0.60

TABLE VIII

Specimen #8

T	I	$\Delta_1(T)$	$\frac{\Delta_1(T)}{\Delta_1(0)}$	$\frac{T}{T_{c_1}}$	$\Delta_2(T)$	$\frac{\Delta_2(T)}{\Delta_2(0)}$	$\frac{T}{T_{c_2}}$
°K		μev			μ		
0.33	1.1×10^{-2}	278	1.00	0.18	178	0.96	0.27
0.35	1.1×10^{-2}	282	1.01	0.19	178	0.96	0.29
0.35	1.1×10^{-2}	276	0.99	0.19	179	0.97	0.29
0.45	1.1×10^{-2}	279	1.00	0.24	181	0.98	0.37
0.50	1.0×10^{-2}	281	1.00	0.27	185	1.00	0.41
0.55	1.3×10^{-2}	280	1.00	0.30	185	1.00	0.45
0.60	1.6×10^{-2}	280	1.00	0.32	185	1.00	0.49
0.65	2.0×10^{-2}	286	1.02	0.35	184	1.00	0.53
0.70	2.4×10^{-2}	270	0.97	0.39	180	0.97	0.57
0.80	4.2×10^{-2}	265	0.95	0.43	150	0.81	0.66
0.90	6.4×10^{-2}	274	0.98	0.49	146	0.79	0.74
1.00	1.3×10^{-1}	258	0.92	0.54	108	0.58	0.82
1.10	2.0×10^{-1}	234	0.84	0.60	29	0.16	0.90

The experimental variation of the tunnel current with temperature is shown in Figures 16, 17, and 18, along with the equation

$$I = 1.33 \left(\frac{T}{\Delta}\right)^{1/2} e^{-\Delta/T} . \qquad (4)$$

The theoretical values of I were calculated using a value of Δ = 0.20 milli-electronvolts (mev). The variation of the energy gaps with temperature is shown in Figures 20, 21, 22, and 23, along with the theoretical curve plotted from values calculated by Muhlschlegel (1959).

C. Discussion of Results

The data on the energy gap temperature variation were obtained principally as a check on the temperature of the specimen. The form of this variation is given by the BCS theory and has been well verified experimentally. By plotting graphs of $\frac{\Delta(T)}{\Delta(0)}$, we can easily see if there is any great discrepancy between the temperature of the germanium resistance thermometer and the tunnel junction itself. From Figures 20 to 23, it can be seen that no such discrepancy exists. Keeping in mind that any of the energy gap measurements have a possible error of 30 micro-electronvolts (μev), the results shown on the graphs do agree with the theoretical curve.

However, there was one exception. From the gap photographs

FIGURE 16

Graph showing variation of tunnel current with temperature for specimens #1, #2, and #3.

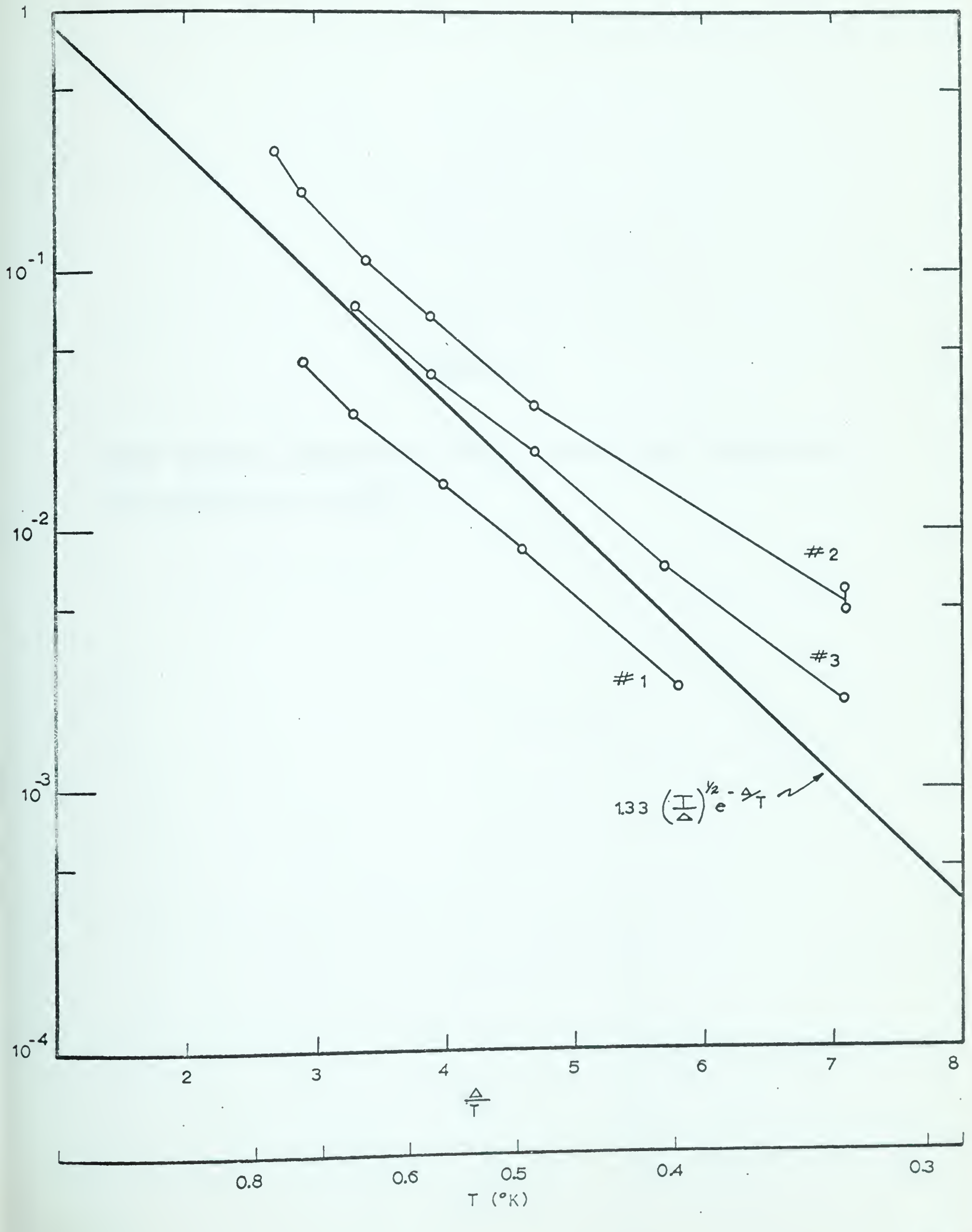
1
10^{-1}
10^{-2}
10^{-3}
10^{-4}
#1
#2
#3
$1.33\left(\frac{T}{\Delta}\right)^{1/2} e^{-\Delta/T}$
2
3
4
5
6
7
8
$\frac{\Delta}{T}$
0.8
0.6
0.5
0.4
0.3
T (°K)

FIGURE 17

Graph showing variation of tunnel current with temperature for specimens #5 and #6.

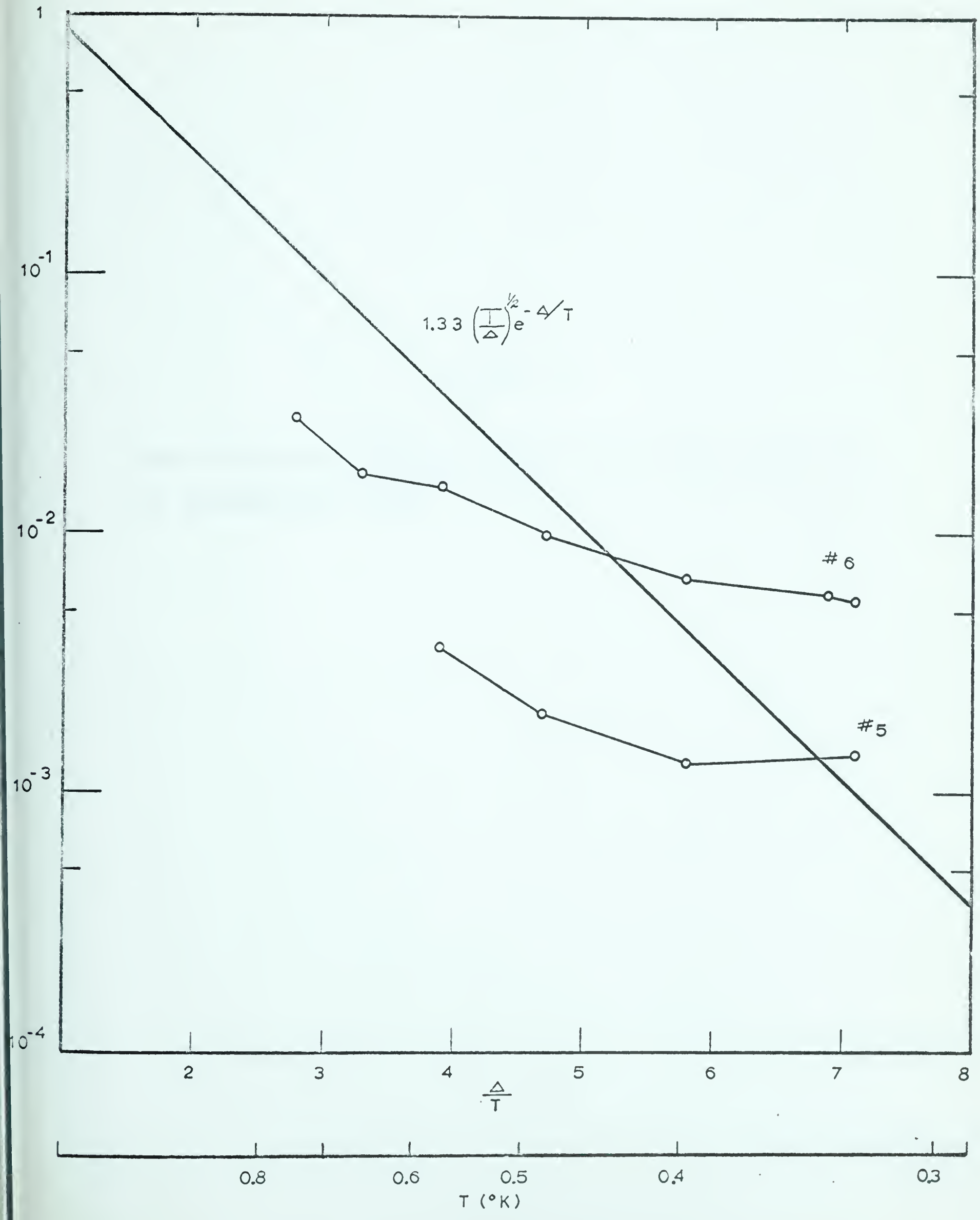
1
10^{-1}
10^{-2}
10^{-3}
10^{-4}
$1.33\left(\frac{T}{\Delta}\right)^{1/2} e^{-\Delta/T}$
#6
#5
2
3
4
5
6
7
8
$\frac{\Delta}{T}$
0.8
0.6
0.5
0.4
0.3
T (°K)

FIGURE 18

Graph showing variation of tunnel current with temperature for specimens #7 and #8.

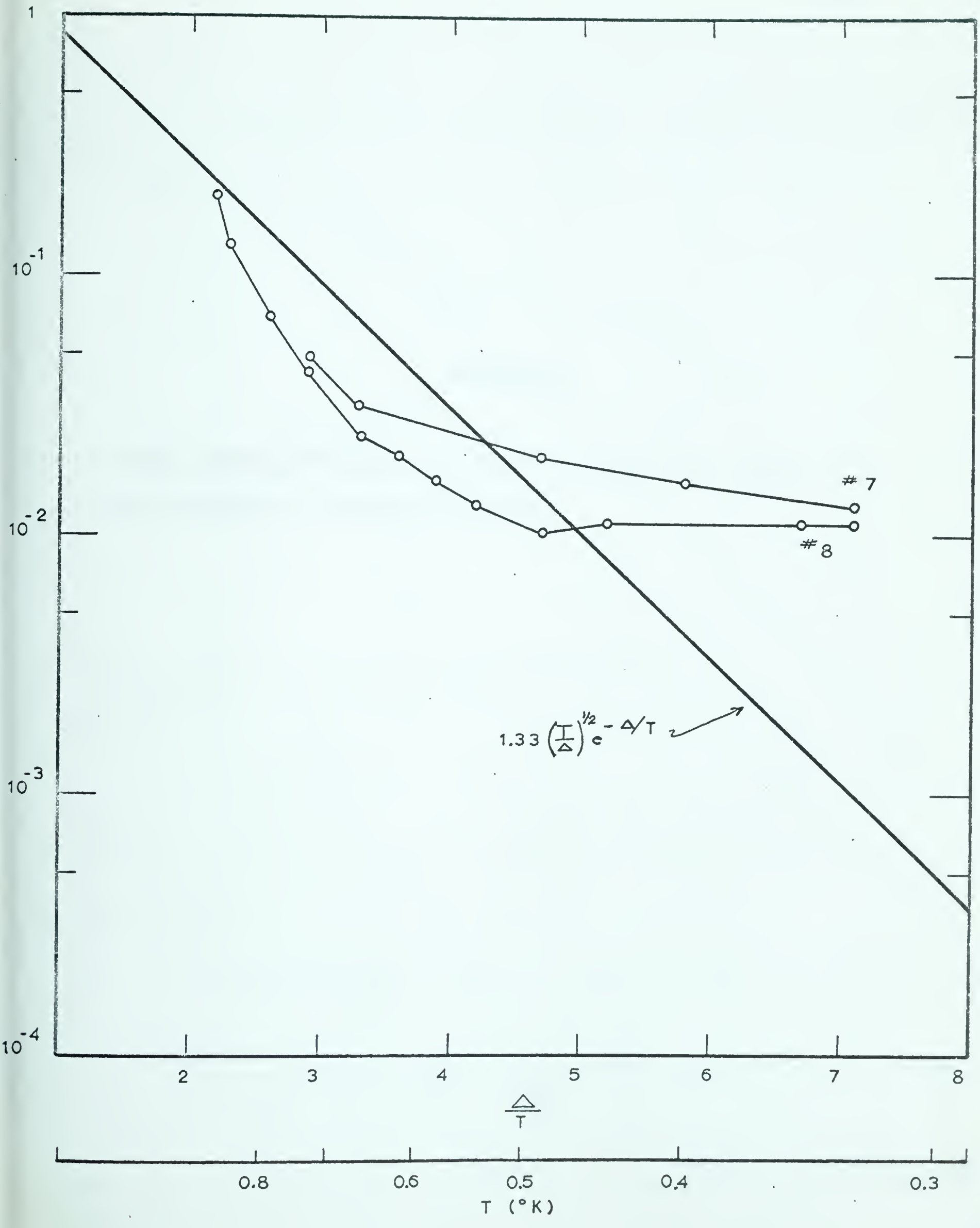
1
10^{-1}
10^{-2}
10^{-3}
10^{-4}
7
8
$1.33\left(\frac{T}{\Delta}\right)^{1/2} e^{-\Delta/T}$
2
3
4
5
6
7
8
$\frac{\Delta}{T}$
0.8
0.6
0.5
0.4
0.3
T (°K)

FIGURE 19

Graph showing variation of tunnel current with temperature as obtained by Rogers and Giaever.

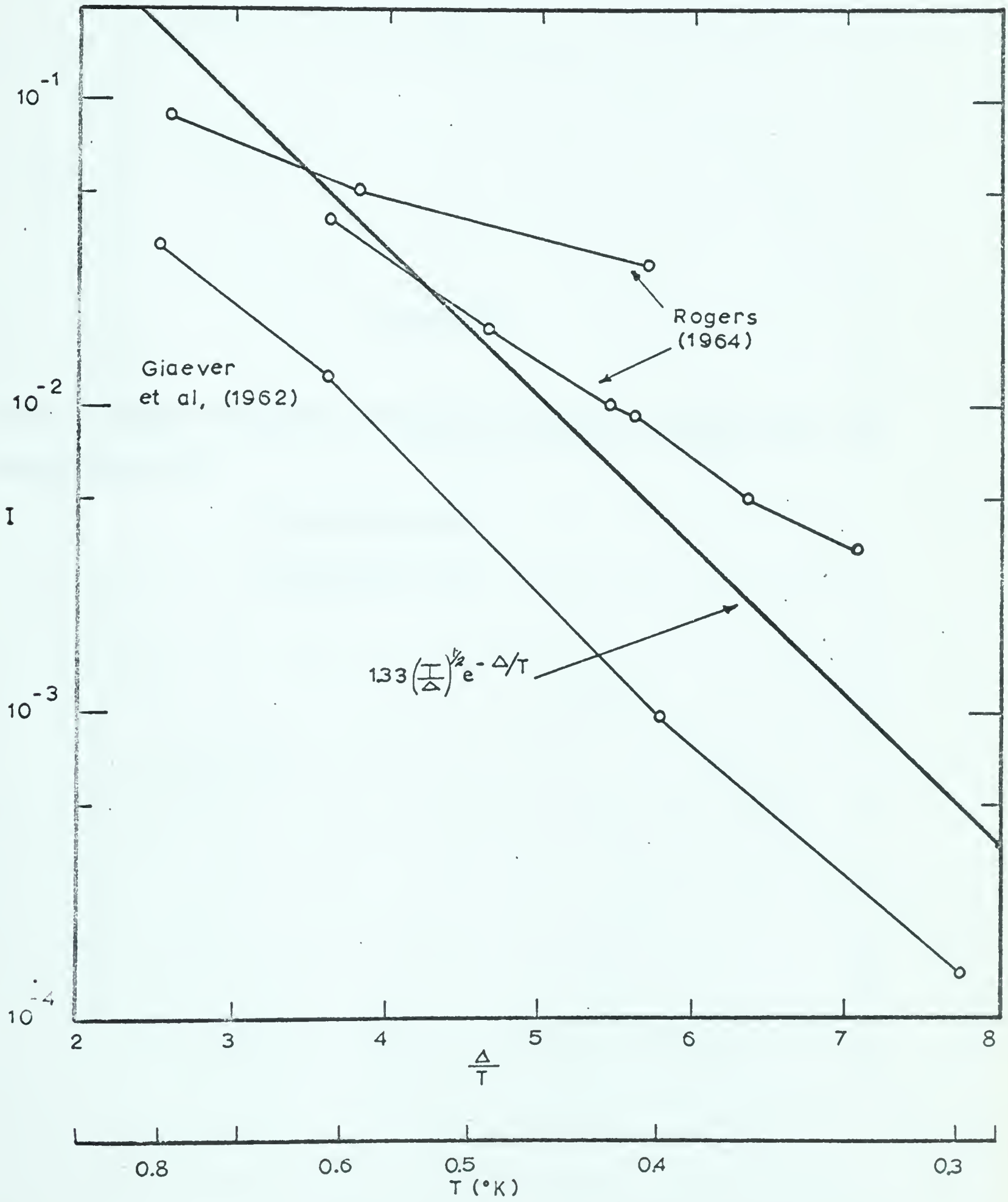
10^{-1}
10^{-2}
10^{-3}
10^{-4}
I
Giaever
et al, (1962)
Rogers
(1964)
$1.33\left(\frac{T}{\Delta}\right)^{1/2} e^{-\Delta/T}$
2
3
4
5
6
7
8
$\frac{\Delta}{T}$
0.8
0.6
0.5
0.4
0.3
T (°K)

FIGURE 20

Graph showing variation of superconducting energy gap with temperature for

a) Specimen #1

b) Specimen #2

(a)

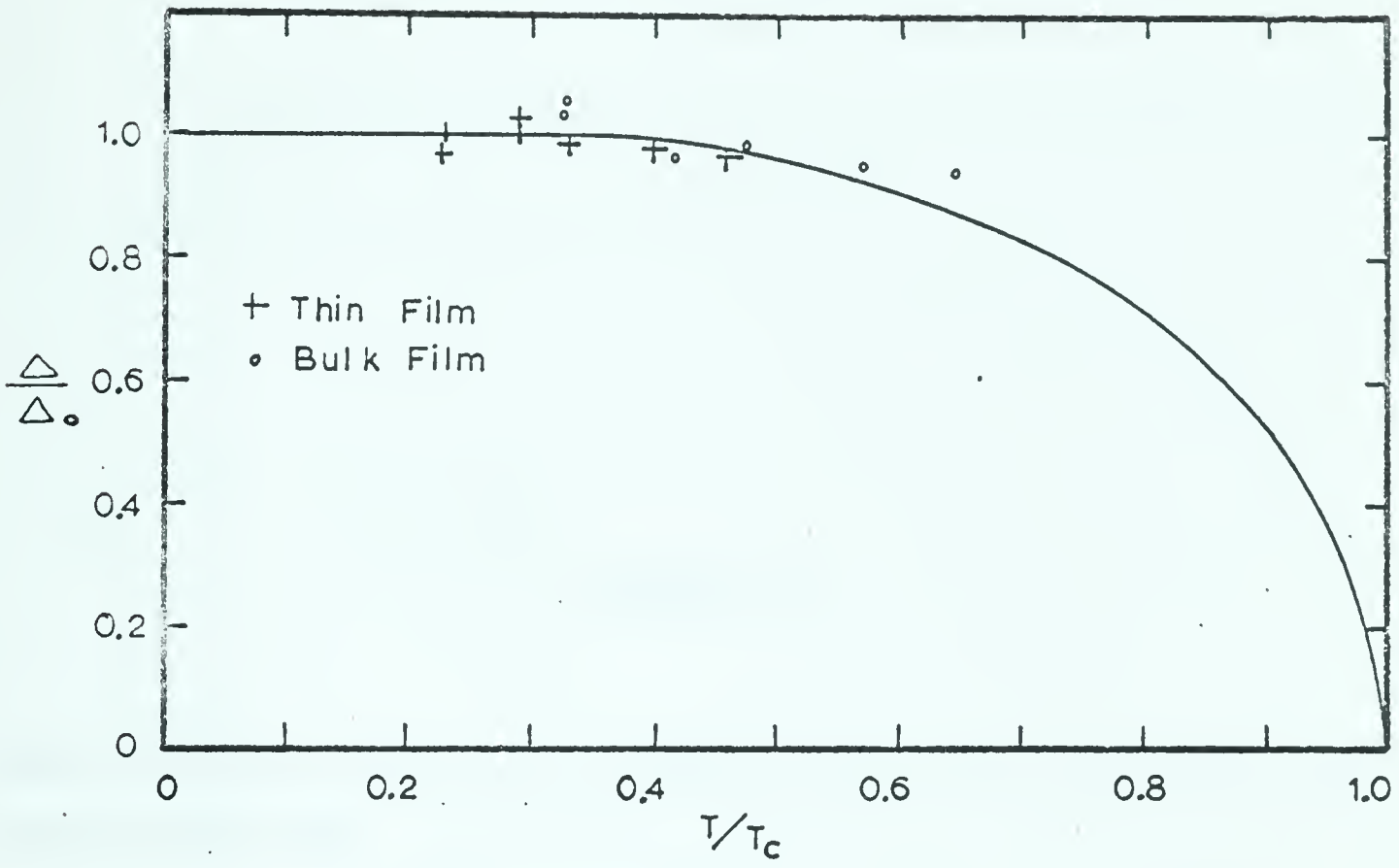
1.0
0.8
0.6
0.4
0.2
0
0
0.2
0.4
0.6
0.8
1.0
+ Thin Film
∘ Bulk Film
Δ/Δ₀
T/Tc

(b)

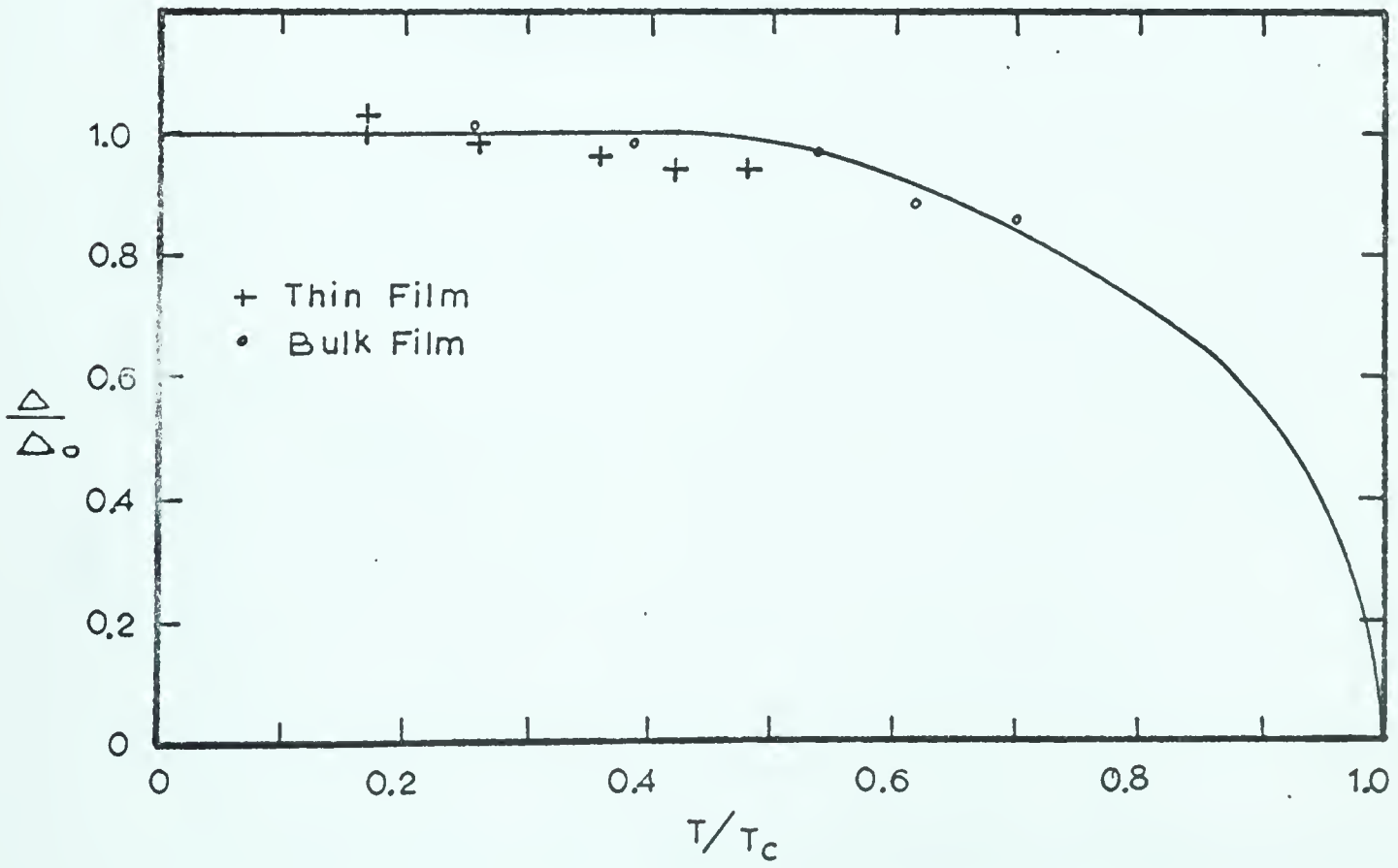
1.0
0.8
0.6
0.4
0.2
0
0
0.2
0.4
0.6
0.8
1.0
+ Thin Film
• Bulk Film
Δ/Δ₀
T/Tc

FIGURE 21

Graph showing variation of superconducting energy gap with temperature for

a) Specimen #3

b) Specimen #5

(a)

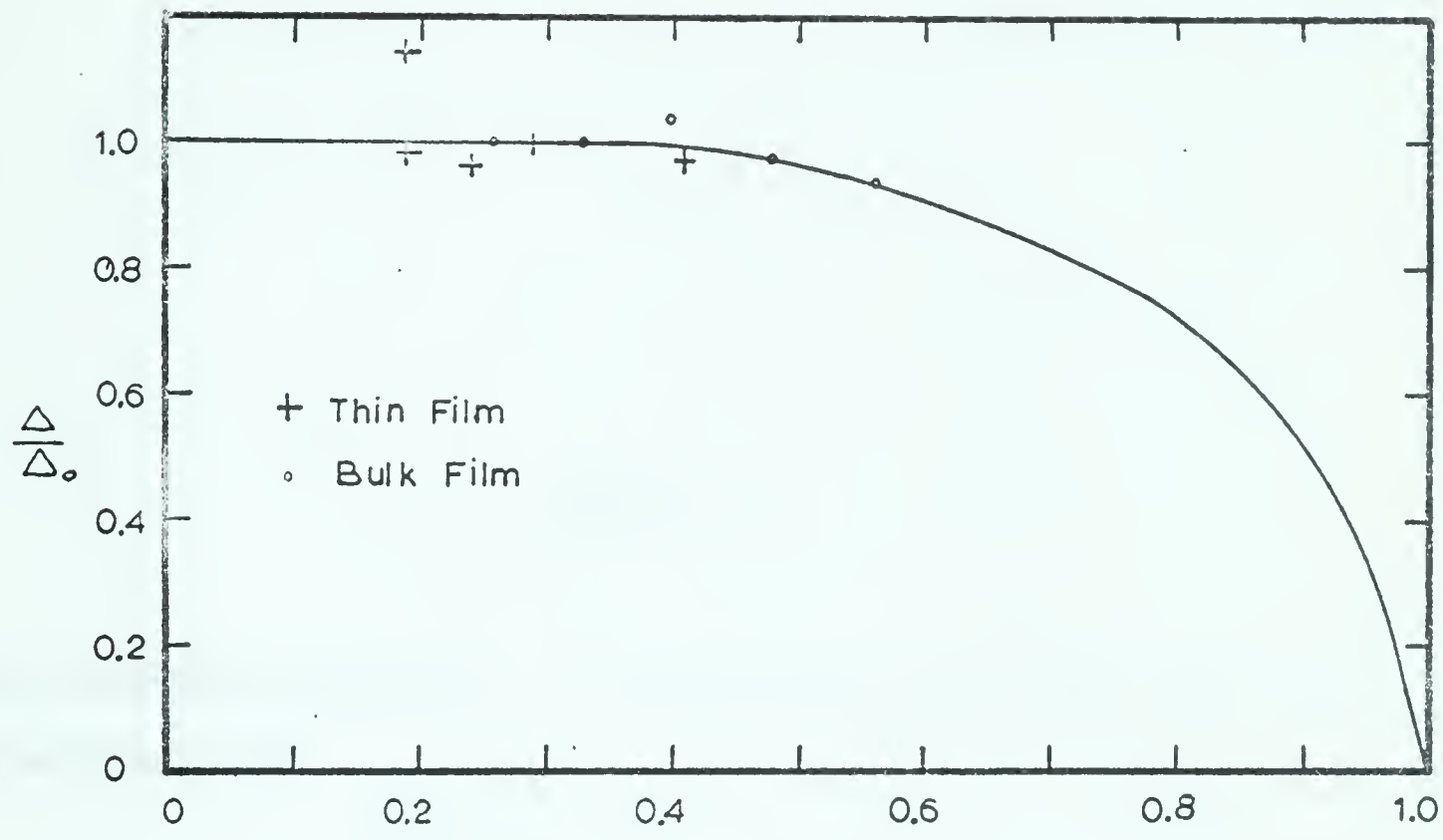
1.0
0.8
0.6
0.4
0.2
0
Δ/Δ₀
+ Thin Film
∘ Bulk Film
0
0.2
0.4
0.6
0.8
1.0
T/Tc

(b)

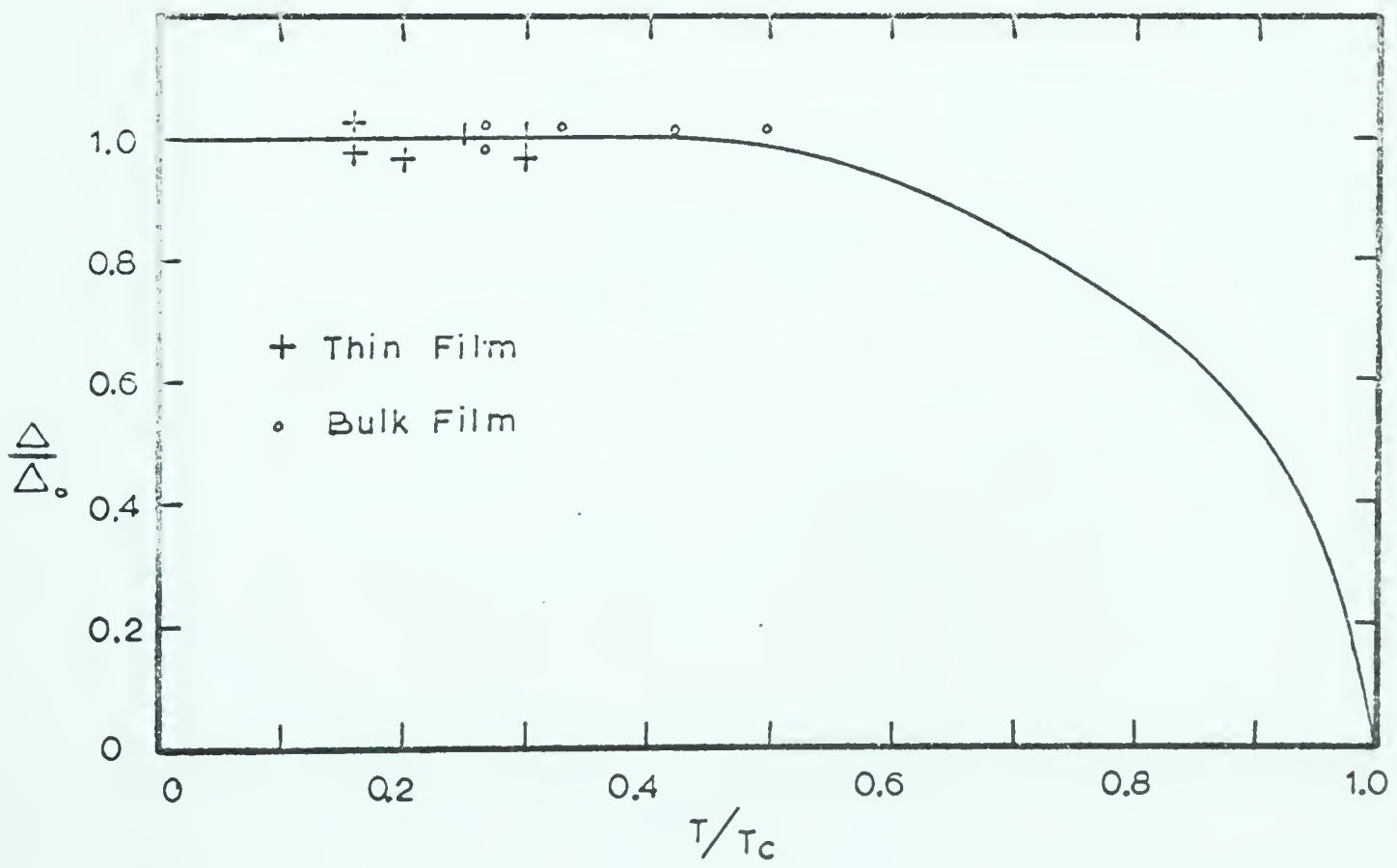
1.0
0.8
0.6
0.4
0.2
0
Δ/Δ₀
+ Thin Film
∘ Bulk Film
0
0.2
0.4
0.6
0.8
1.0
T/Tc

FIGURE 22

Graph showing variation of superconducting energy gap with temperature for

a) Specimen #6

b) Specimen #7

(a)

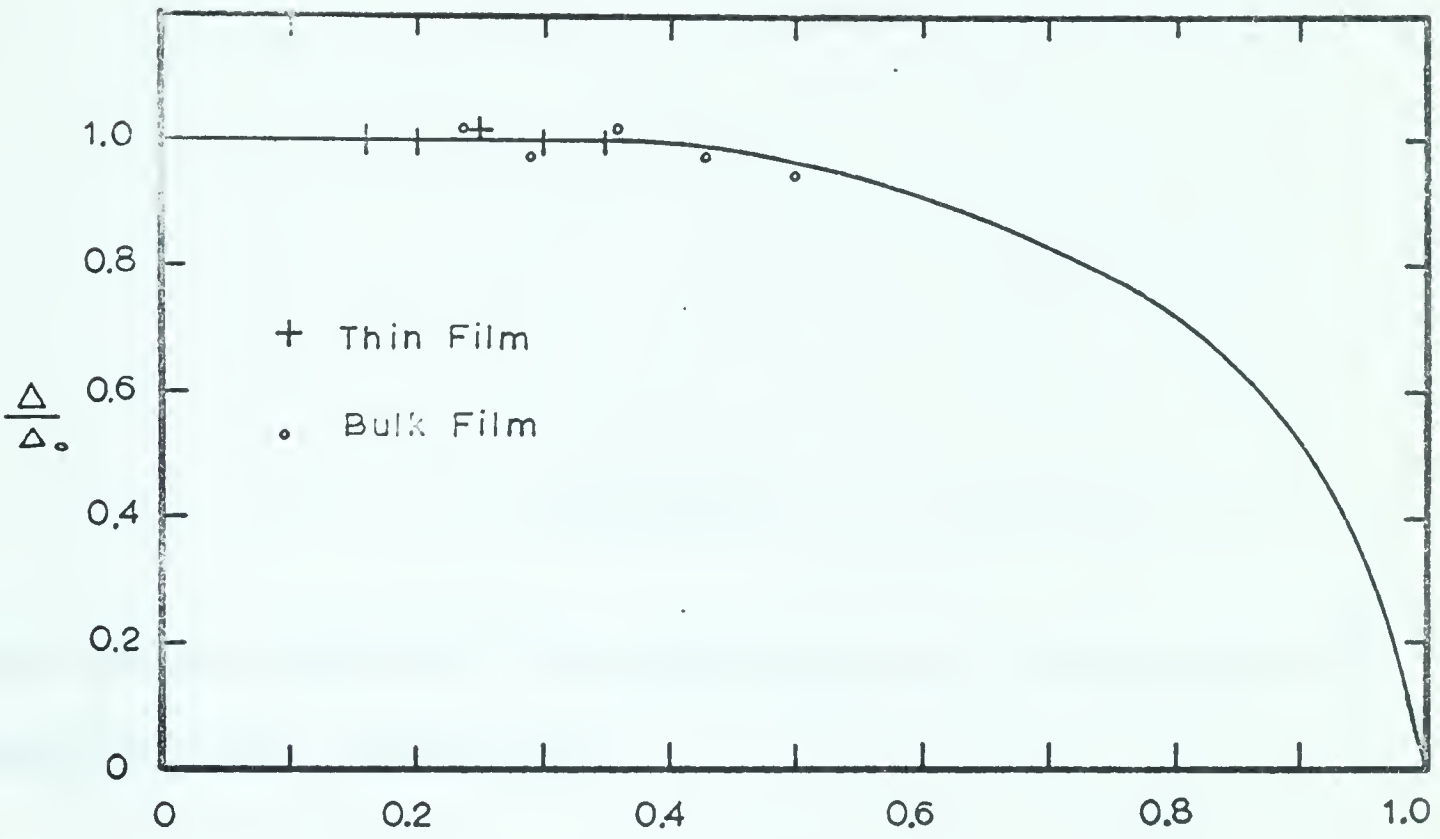
1.0
0.8
0.6
0.4
0.2
0
Δ/Δ₀
+ Thin Film
° Bulk Film
0
0.2
0.4
0.6
0.8
1.0
T/Tc

(b)

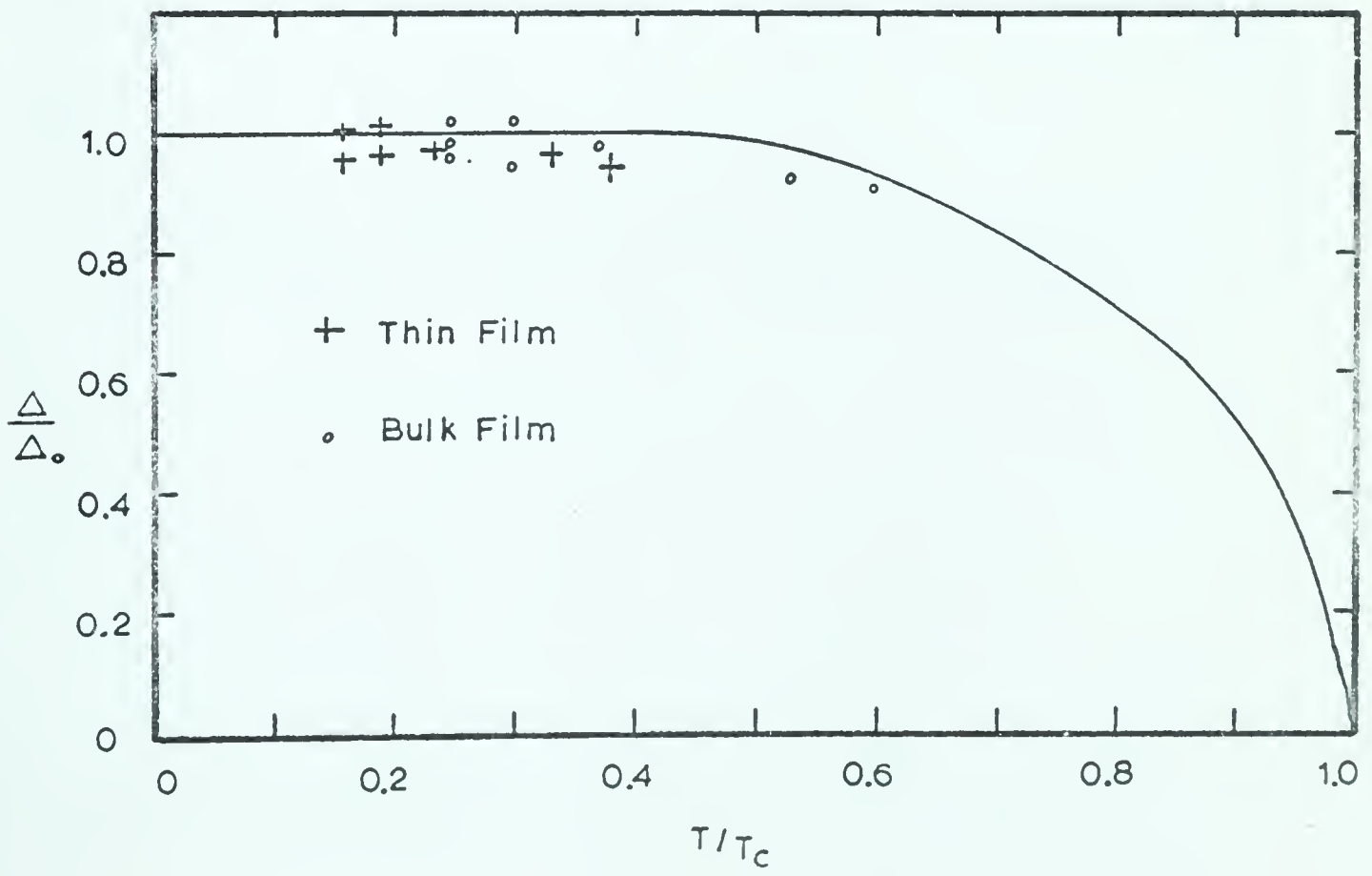
1.0
0.8
0.6
0.4
0.2
0
Δ/Δ₀
+ Thin Film
° Bulk Film
0
0.2
0.4
0.6
0.8
1.0
T/Tc

FIGURE 23

Graph showing variation of superconducting energy gap with temperature for Specimen #8.

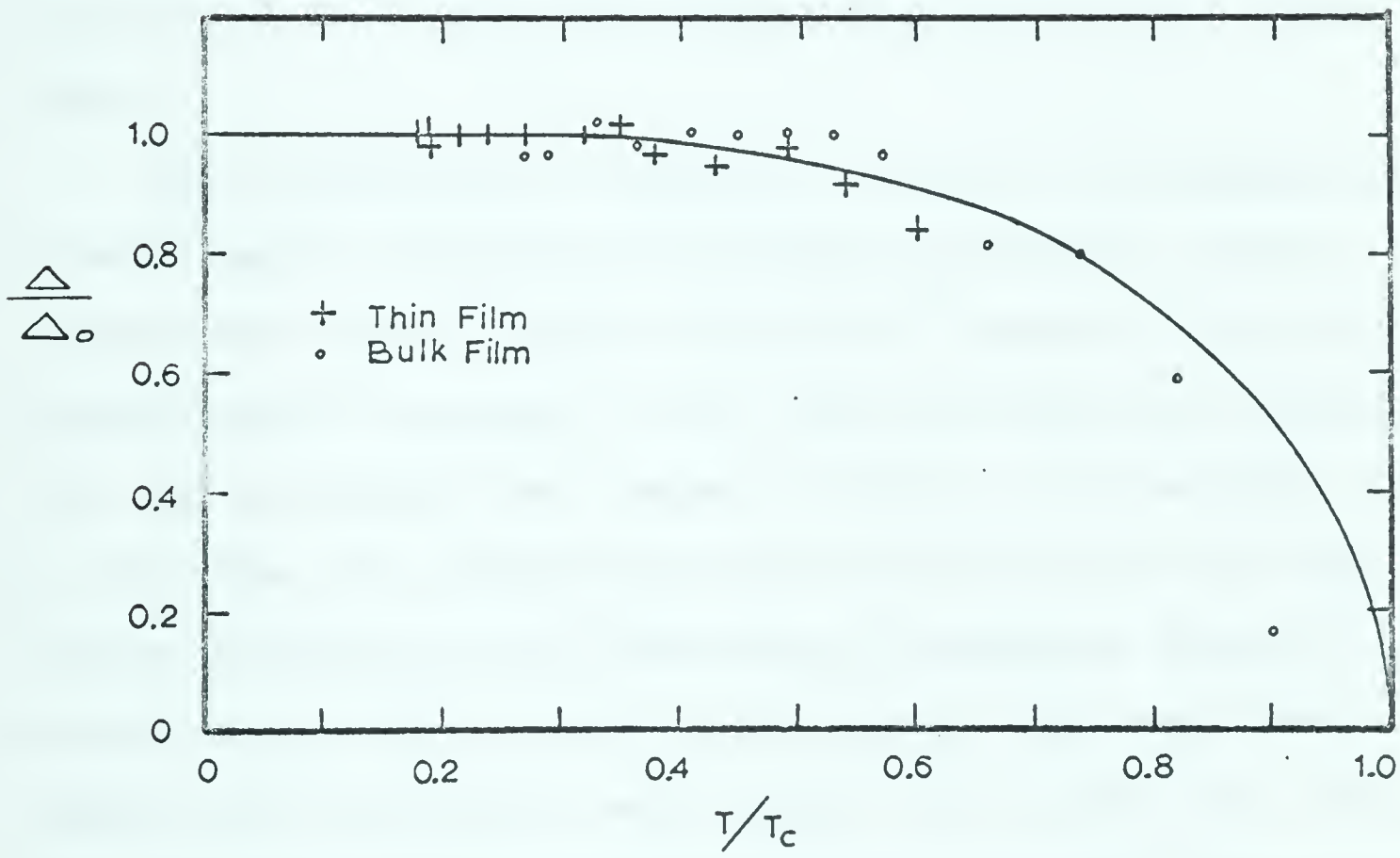
1.0
0.8
0.6
0.4
0.2
0
Δ/Δ₀
+ Thin Film
° Bulk Film
0
0.2
0.4
0.6
0.8
1.0
T/Tc

at 0.33°K for specimen #8, the energy gap in the thick film was calculated to be 170 μev. Using this value as $\Delta_2(o)$ in the values of $\frac{\Delta_2(T)}{\Delta_2(o)}$, it was found that the straight line portion of the function was at a value of $\frac{\Delta(T)}{\Delta(o)} = 1.1$. The values used to plot Figure 23 were calculated using a value of $\Delta_2(o) = 185$ ev which gives a much better fit with the theoretical curve. This value of Δ_2 is also in much better agreement with other values obtained for the thick film.

This difference in values of $\Delta_2(o)$ for specimen #8 is most easily explained by assuming bad thermal contact between the tunnel junction and the He^3 chamber. The photographs used to calculate $\Delta(o)$ were the first ones taken. With the postulated poor thermal contact, it is possible that at this time the junction had not cooled down to the temperature indicated by the resistance thermometer which is mounted on the He^3 chamber itself. By the time the other temperature measurements were taken, the junction had cooled down, and the problem of thermal contact is much less evident in heating the speciment to get the higher temperature measurements.

The above theory is also supported by the behaviour of the tunnel current shown in Figure 18. The experimental results should at least follow a straight line parallel to the theoretical curve. The points shown for specimen #8 were

taken in order from right to left as they appear on the graph. Thus the later measurements (higher temperature ones) are not in excellent agreement with theory but they are much closer than the first two. The first two current values correspond to a junction temperature of around 0.6°K. Assuming a bulk $\Delta_2(o)$ equal to 185 μev, at this temperature the energy gap should be about 170 to 175 μev, which, taking into account the experimental error, is very close to the 170 μev actually calculated.

From Figures 16, 17, and 18, it can be seen that specimens 1, 2, and 3 gave results in quite good agreement with theory, but that the other specimens did not. Specimens 5 to 8 do all show the same type of disagreement in that the low temperature values (which were the first readings taken in all cases) are too high, indicating that the junction temperature is not as low as that of the resistance thermometers. In all cases the results do seem to come closer to the theoretical curve at higher temperatures.

There remains the possibility that the results from specimens 5 to 8 show the proper behaviour while the first three are wrong. However, this is very unlikely since the previous work done on the subject agrees with the theoretical prediction, as can be seen from Figure 19, which shows Rogers' results along with some obtained from I-V characteristics measured and published by Giaever.

It has been previously assumed in this laboratory that a vacuum of approximately 1 x 10^{-6} mm. of mercury was necessary in the experimental chamber, and that in cases of bad thermal contact between specimen and He^3 chamber, that an insufficient vacuum was the cause. This explanation no longer appears valid, since the readings for specimens 1, 2, and 3 were taken with a pressure in the experimental chamber of 6 to8 x 10^{-6} mm, while for specimens 5 to 8 it was in the range 1 to 2 x 10^{-6} mm. of mercury. The bad thermal contact seems to lie entirely in the Wood's metal joint between the specimen chamber and the He^3 can.

CHAPTER VI

BROADENING OF THE GAP-EDGE SINGULARITY

A. Theoretical Modifications of the BCS Density of States

Earlier workers in the field of electron tunneling noted that the slope of the I-V characteristic at the current jump is less than expected even after the fact that the measurements are taken at a temperature $T > 0^{\circ}K$ is taken into account. The general solution has been to follow Hebel and Schlichter (1959) in assuming that the energy levels in a superconductor are not sharply defined but have a finite width. We take this width to be δ and adjust δ to give the best fit with the experimental results.

The density of states obtained with energy levels of finite width (ρ_{HS}) is given by

$$\rho_{HS} = \frac{1}{2\delta} \int_{E-\delta}^{E+\delta} (\quad) \, dE' \qquad (1)$$

After integration the result is

$$\rho_{HS} = 0 \qquad \text{for} \quad |E| < \Delta - \delta$$

$$\rho_{HS} = \frac{1}{2\delta} \left[(E+\delta)^2 - \Delta^2 \right]^{1/2} \qquad \text{for} \quad \Delta - \delta < |E| < \Delta + \delta \qquad (2)$$

$$\rho_{HS} = \frac{1}{2\delta} \left\{ \left[E + \delta \right]^2 - \Delta^2 \right\}^{1/2} - \left[(E-\delta)^2 - \Delta^2 \right]^{1/2}$$

$$\text{for} \quad |E| > \Delta + \delta$$

The most important effect of this modification is to remove the singularity in the BCS density of states.

Rogers (1964) produced a similar density of states by merely truncating the BCS density of states, without trying to find any physical justification or explanation. He replaces the BCS function

$$G = RP\left\{1-\left(\frac{\Delta}{E}\right)^2\right\}^{-1/2}$$

by the function

$$\begin{aligned} G_s &= 0 && x < -\alpha \\ G_s &= (2\alpha)^{-1/2} && -\alpha < x < \alpha \\ G_s &= (2x)^{-1/2} && \alpha < x \ll 1 \end{aligned} \qquad (3)$$

where $x = \frac{E-\Delta}{\Delta}$ represents energy measured from the gap edge in units of Δ. Using the truncated function G_s, the normalized dynamic conductance for a symmetric tunnel junction is

$$\sigma = \frac{1}{2x} \quad \text{for} \quad 2\Delta(1-\alpha) < V < 2\Delta . \qquad (4)$$

B. Experimental Results

Although the junctions used in the present experiments are not really symmetric, used has been made of Rogers' result, $\sigma = \frac{1}{2\alpha}$, in order to compare present work with previous work. The results are shown in Table IX and Table X. The first of these tables shows the values of α

TABLE IX

Values of Gap-edge Broadening Parameter

Specimen	Reference	α
Al-Al 26	Adler	0.10
Al-Al 34	Rogers	0.03
Al-Al 42	Rogers	0.03
Al-Al	Giaever (1961)	0.02
Al-Al	Giaever (1961)	0.05
Sn-Sn	Giaever (1961)	0.03
Al #6	This work	0.03
Al #7	This work	0.04

TABLE X

Temperature Variation of α

Temp. (°K)	α
0.33	0.03 ± 0.01
0.40	0.03 ± 0.01
0.40	0.03 ± 0.01
0.50	0.03 ± 0.01
0.60	0.03 ± 0.01
0.70	0.04 ± 0.01

obtained from specimens #6 and #7, along with the results of previous workers. All of the values from this laboratory (Adler, Rogers, this work) are at temperatures of 0.33 to 0.35°K. Table X gives the results obtained from specimen #8 for which the value of α was obtained for the different temperatures shown in the table. These results show the value of α to be constant within the limits of our experimental error.

C. Discussion of Results

Very little can be concluded from the results of Section B, aside from the fact that the slope of a tunnel junction I-V characteristic at the current jump does not appear to vary with temperature, at least not in the range 0.3 to 0.8°K. However, in order to state even this definitely, more sensitive apparatus is necessary. One way of providing this would be to use a galvanometer preamplifier on both vertical and horizontal outputs from the curve tracer.

This apparent lack of temperature variation throws an interesting light on the Hebel-Schlichter gap-smearing mechanism. Presumably the finite level width can be linked to lifetime effects through the uncertainty principle ($\Delta \cdot \tau \sim \hbar$). It is to be expected that the lifetime τ would decrease with rising temperature, and hence that δ would increase with rising temperature. Such an increase in δ should lead to a

decreasing slope of the I-V characteristic as the temperature rises, but no such variation is found experimentally.

CHAPTER VII

CONCLUSIONS

A. Conclusions

In the introduction, it was said that the present experiments were intended to investigate:

1. The shape resonance theory of Blatt and Thompson,
2. Use of tunnel junctions as thermometers,
3. The temperature variation of the broadening of the gap-edge singularity.

The conclusions which can be drawn from the results of these experiments are stated below:

1. No real verification was found for shape resonances. The results did indicate that the increase of the energy gap in thin films is due to differential contraction of the film and the glass substrate as the specimen is cooled from room temperature.
2. Tunnel junctions can be used as thermometers. Calculation of the tunnel current I showed that some of our specimens were not at the temperature indicated by the germanium resistance thermometer.

3. The results on energy gap smearing lead to the conclusion that the slope of the I-V characteristic at the current jump does not vary with temperature.

B. Proposals for Further Work

Further work on variation of the superconducting energy gap should be done on still thinner films in an attempt to verify the sharp decrease in the energy gap around 15 to 20 A. Evidence of such a decrease would be very good verification of Toxen's strain theory. Similar work could also be done with indium thin films in which Toxen's exact results (theoretical) could be checked for films much thinner than those with which he worked.

Further work should also be done on the smearing of the energy gap, with more sensitive apparatus. If the experimental error can be reduced to 1 or 2 % from the present 10%, temperature variation, or its absence, could be found more definitely than can be done with the present apparatus.

BIBLIOGRAPHY

Adler, J.G., 1963. Electron Tunneling into Superconductors. Doctoral Thesis, University of Alberta

Bardeen, J., Cooper, L.N., and Schrieffer, J.R., 1957. Phys. Rev. 108, 1175.

Blatt, J.M., 1964. Theory of Superconductivity, Academic Press, New York and London.

Blatt, J.M., and Thompson, C.J., 1963 a. Phys. Rev. Letters 10, 332.

Blatt, J.M., and Thompson, C.J., 1963 b. Physics Letters 5, 6.

Dingle, R.B., 1950. Proc. Roy. Soc. A201, 545.

Fuchs, K., 1938. Proc. Camb. Phil. Soc. 34, 100.

Giaever, I., 1960. Phys. Rev. Letters 5, 147.

Giaever, I., 1960. Phys. Rev. Letters 5, 464.

Giaever, I., Hart, H.R., and Megerle, K., 1962. Phys. Rev. 126, 941.

Hebel, L.C., and Schlichter, C.P., 1959. Phys. Rev. 113, 1504.

Jennings, L.D., and Swenson, C.A., 1958. Phys. Rev. 112, 31.

Lock, J.M., 1951. Proc. Roy. Soc. A208, 391.

Lovell, A.C.B., 1936. Proc. Roy. Soc. A157, 311.

Muhlschlegel, B., 1959. Z. Phys. 155, 313.

Nicol, J., Shapiro, S., and Smith, P.H., 1960.
Phys. Rev. Letters 5, 461.

Rogers, J.S., 1964. Phonon Effects in Electron Tunneling into Superconductors. Doctoral Thesis, University of Alberta.

Rogers, J.S., Adler, J.G., and Woods, S.B., 1964.
Review of Scientific Instruments 35, 208.

Shapiro, S., Smith, P.H., Nicol, J., Miles, J.L., and Strong, P.F., 1962. IBM Jour. 6, 34.

Toxen, A.M., 1961. Phys. Rev. 123, 442.

Zavaritskii, N.V., 1951.
Doklady Akad. Nauk U.S.S.R. 78, 665.